hydrology

MDPI

Article

Seasonal Precipitation Variability and Its Association with Atmospheric Teleconnections in the Fez-Meknes Region, Morocco: NAO, EAP and WeMO

Ridouane Kessabi [1], Mohamed Hanchane [1], Gaetano Pellicone [2], Nir Y. Krakauer [3,4], Alessandra De Marco [5] and Tommaso Caloiero [6,*]

1 Department of Geography, Laboratoire Territoire Patrimoine et Histoire, FLSH Dhar El-Mehraz, Sidi Mohamed Ben Abdellah University, Fez 30050, Morocco; ridouane.kessabi@usmba.ac.ma (R.K.); mohamed.hanchane@usmba.ac.ma (M.H.)
2 National Research Council of Italy, Institute for Agriculture and Forest Systems in the Mediterranean (CNR-ISAFOM), Via Cavour 4/6, 87036 Rende, Italy; gaetano.pellicone@cnr.it
3 Department of Civil Engineering, The City College of New York, New York, NY 10031, USA; nkrakauer@ccny.cuny.edu
4 Department of Earth and Environmental Sciences, The City University of New York Graduate Center, New York, NY 10016, USA
5 Territorial Research Area of Cosenza, National Research Council of Italy, Via Cavour 4/6, 87036 Rende, Italy; alessandra.demarco@cnr.it
6 Institute of Geosciences, National Research Council of Italy (CNR-GEO), Via Cavour 4/6, 87036 Rende, Italy
* Correspondence: tommaso.caloiero@cnr.it

Abstract

This study investigated seasonal precipitation variability in the economically and agriculturally important Fez-Meknes region and its relationship with major atmospheric circulation patterns, namely the North Atlantic Oscillation (NAO), Western Mediterranean Oscillation (WeMO), and East Atlantic Pattern (EAP), using data from 1961–2019. Results showed strong seasonal associations between precipitation and the three teleconnection indices. The NAO showed the strongest relationships with autumn and winter precipitation, the EAP with spring precipitation and, to a lesser extent, summer precipitation, while the WeMO was primarily associated with autumn rainfall. Correlations were generally negative, indicating that positive phases of these indices tend to reduce precipitation, whereas negative phases favor wetter conditions. During negative NAO phases, autumn precipitation increased by 7–13% and winter precipitation by 34–57%, while positive phases produced decreases of 17–32% and 26–37%, respectively. EAP-related spring precipitation anomalies ranged from −16% to −33% during positive phases and +12% to +24% during negative phases, while WeMO affected autumn rainfall by 9–17%. Wavelet analysis further highlighted the temporal variability of these relationships, revealing significant annual-scale coherence and multiyear periodicities, including approximately 2-, 6–8-, and 12-year bands for NAO-related variability, as well as lower-frequency 7–10-year and >16-year signals for WeMO at selected stations. The results improve understanding of regional precipitation variability and provide useful information for drought assessment and water-resource planning.

Keywords: precipitation; teleconnections; NAO; EAP; WeMO; Morocco

Check for updates

Academic Editor: Yanfang Sang

Received: 8 September 2026
Revised: 27 October 2026
Accepted: 28 October 2026
Published: 30 October 2026

Copyright: © 2026 by the authors. Licensee MDPI, Basel, Switzerland. This article is an open access article distributed under the terms and conditions of the Creative Commons Attribution (CC BY) license.

1. Introduction

North Africa is considered one of the hot spots of anthropogenic climate change, with rising temperatures and declining precipitation [1]. Close to the largest desert on

Earth, precipitation plays a vital role in the agriculture and economy of Morocco. Along with neighboring countries, it is dominated by arid and semi-arid climates where rainfall variability is very high. As an example, in 2024 a severe drought hit the country for the sixth consecutive year [2,3], resulting in an unprecedented shortage in water reservoirs (dry dams and lakes) and triggering public protest due to water supply deficits. Cereal production declined by over 40%, increasing import dependence and exposure to international market fluctuations [4,5]. In this context, understanding atmospheric circulation patterns associated with precipitation within this region becomes crucial. Atmospheric teleconnections are interlinked synoptic patterns in the pressure and hence flow fields [6] that often have significant associations with precipitation and temperature variability across distances and locations, typically explored through correlations, principal component analysis (PCA) or empirical orthogonal functions (EOF) [7].

The North Atlantic Oscillation (NAO) is a major driver of climate variability in the northern Atlantic basin, especially in the cold season [8]. The station-based/grid-point based NAO index is conventionally defined as the difference in the standardized atmospheric pressure values between the Azores subtropical high and the Icelandic subpolar low. It is one of the most studied atmospheric oscillation modes [9,10]. Information on its impacts goes back centuries, especially in Scandinavia [11]. It is one of the major drivers of seasonal to inter-decadal variability in global atmospheric circulation [8]. Morocco's climate is strongly affected by this oscillation [1–3]. Overall, the NAO presents two phases, positive and negative. The positive phase is characterized by a strengthening of the two centers of atmospheric action (the Azores High and the Icelandic Low). In this case, the westerly winds strengthen over Western Europe, shifting the path of the storms northward and promoting a zonal circulation from west to east. These atmospheric situations favor mild and rainy winters over northwestern Europe, and dry to arid winters over the Mediterranean, including Morocco [12,13]. By contrast, during the negative phase, the two centers of atmospheric action weaken. The Azores High withdraws to a more southerly position in the middle of the Atlantic Ocean and the Icelandic Low is pushed southward by the meandering undulations of the polar Jet Stream. In this case, north-south exchanges become the rule in the North Atlantic. Northern Europe is dominated by high pressure and dry and very cold Arctic air masses (Scandinavian blocking situation as an example) with more snowfall than liquid rain. Under these conditions, the storm track migrates southward, bringing more disturbances, more rain and humidity to the Mediterranean area, including Morocco [14–16]. The effects of the North Atlantic Oscillation on rainfall in Morocco have been investigated by several authors [17–20]. The East Atlantic (EA) pattern considered here corresponds to the formulation of Barnston and Livezey [21] and to the NOAA/CPC EA index. It is characterized by a north–south dipole of geopotential-height anomalies over the North Atlantic, with its main anomaly centers displaced southeastward relative to those of the NAO. This southeastward displacement, together with the stronger subtropical component of the lower-latitude center, makes the EA dynamically distinct from the NAO [22]. During its positive phase (EA+), positive geopotential-height anomalies and enhanced subtropical ridging tend to favor more stable atmospheric conditions over the subtropical eastern North Atlantic and southwestern Europe, and are generally associated with below-average precipitation over southern Europe. The negative phase (EA−) is characterized by the opposite anomaly configuration and is more favorable to cyclonic conditions and moisture transport toward the southwestern Mediterranean. Previous studies indicate that EA− conditions are associated with wetter conditions in Morocco, whereas EA+ conditions are generally linked to precipitation deficits, especially in spring [23,24]. The influence of the EA on Moroccan precipitation has received less attention than that of the NAO, although available studies indicate a significant role, particularly for spring rainfall. The

Western Mediterranean Oscillation (WeMO) is an atmospheric oscillation in the western Mediterranean. It is described by an index measuring the difference in atmospheric pressure between Cadiz (36°28′ N–6°12′ W) in southern Spain and Padua (45°24′ N–11°52′ E) in northern Italy. Proposed by researchers from the climatology group of the University of Barcelona [25], the WeMO index was initially studied to explain the advent of torrential rains in Catalonia and the east of the Iberian Peninsula [26]. It manifests itself in two phases, one positive and the other negative, as is the case for the various atmospheric teleconnections. The positive phase of the WeMO is characterized by high pressure over the Gulf of Cadiz (the Azores arm) and the maritime areas between Morocco and Portugal, and low pressure over northern Italy (Ligurian Sea depression). This favors stable and sunny weather. It is associated with drought in Morocco and Andalusia. During the negative phase, the situation is reversed; the anticyclones of Eastern Europe, infiltrating the Mediterranean, dominate the north of Italy, at the same time as low-pressure cells dominate the Bay of Cadiz. The circulation types that characterize the negative phase draw air from the warm waters of the Western Mediterranean, causing torrential rainfall in the east of Spain and even on the northern coast of Morocco. Few studies have been conducted on the effect of the WeMO oscillation on rainfall in Morocco [27]. One study of the lower Sebou River basin in Morocco on the effects of the Mediterranean oscillation (MO) (an index more specific for the Mediterranean basin than WeMO) on rainfall evidenced a strong MO impact on the December rainfall at the Sidi Slimane station [28].

The climate of Morocco is shaped by interactions between those atmospheric patterns and oscillations, among others, which occur simultaneously. The main purposes of this study are: a) describing the correlations and links between seasonal rainfall within the Fez-Meknes region and the NAO, EAP and WeMO large-scale atmospheric circulation indices; b) presenting spatial and temporal variability of changes in the seasonal rainfall averages according to different phases of those atmospheric indices. The present study focuses specifically on the NAO, EAP, and WeMO because these modes are directly related to the atmospheric variability over the North Atlantic and the western Mediterranean sectors surrounding Morocco. Teleconnection modes involving more remote centers of action, including the Arctic Oscillation (AO), Scandinavian Pattern (SCAN), and El Niño–Southern Oscillation (ENSO), require separate consideration because their pathways of influence may differ and are therefore beyond the scope of the present analysis. The novelty of this study lies not simply in considering all four seasons, but in integrating seasonal correlation patterns, phase-dependent precipitation anomalies, spatial variability across contrasting hydroclimatic environments, and time-frequency relationships within a common analytical framework. This approach enables the simultaneous evaluation of the strength, spatial coherence, magnitude, and temporal stability of NAO-, EAP-, and WeMO-related precipitation variability.

2. Study Area

The Fez-Meknes region is one of the most important regions of Morocco (Figure 1a). It occupies an area of 40,000 km^2, the size of a small country, with a population estimated at 4.3 million distributed among eight provinces [29]. It includes large cities such as Fez and Meknes and medium-sized cities such as Taza, along with extensive villages and farmland. According to the Köppen-Geiger climate classification [30], the climate of this study area is Mediterranean Csa on the west and northwest side of the region, mountainous Csa climate in the Atlas and Rif mountains, and dry and continental BWk in the leeward of the mountain to the east and south-east. Annual precipitation averages range from 741 mm to 423 mm. The most humid climate is found on the mountain peaks of the Middle Atlas and the Rif mountains (988 mm in Ifrane), while arid to semi-arid climates characterize the South-East,

with only 161 mm in Missour (Figure 1d). The wet season starts around October and lasts until April and May, depending on the sub-zone and area. The dry season persists between May and September. The study area has important water resources, especially the Sebou Basin, which is the richest watershed nationally, with an annual average water discharge of 6 billion cubic meters [31]. These water resources were exploited through the construction of several dams (Al-Wahda Dam, Idris I Dam, etc.) to mobilize water resources for the irrigation of important areas in the Gharb Plain and the provision of drinking water to villages and cities. Rainfall also guarantees an important percentage of the grain yield in the case of an average or good season [32]. All of this makes the study area an important agricultural asset along with its resources of forests and meadows, but it is vulnerable to climate variability, whose intensity is expected to increase in the coming years and decades [33,34].

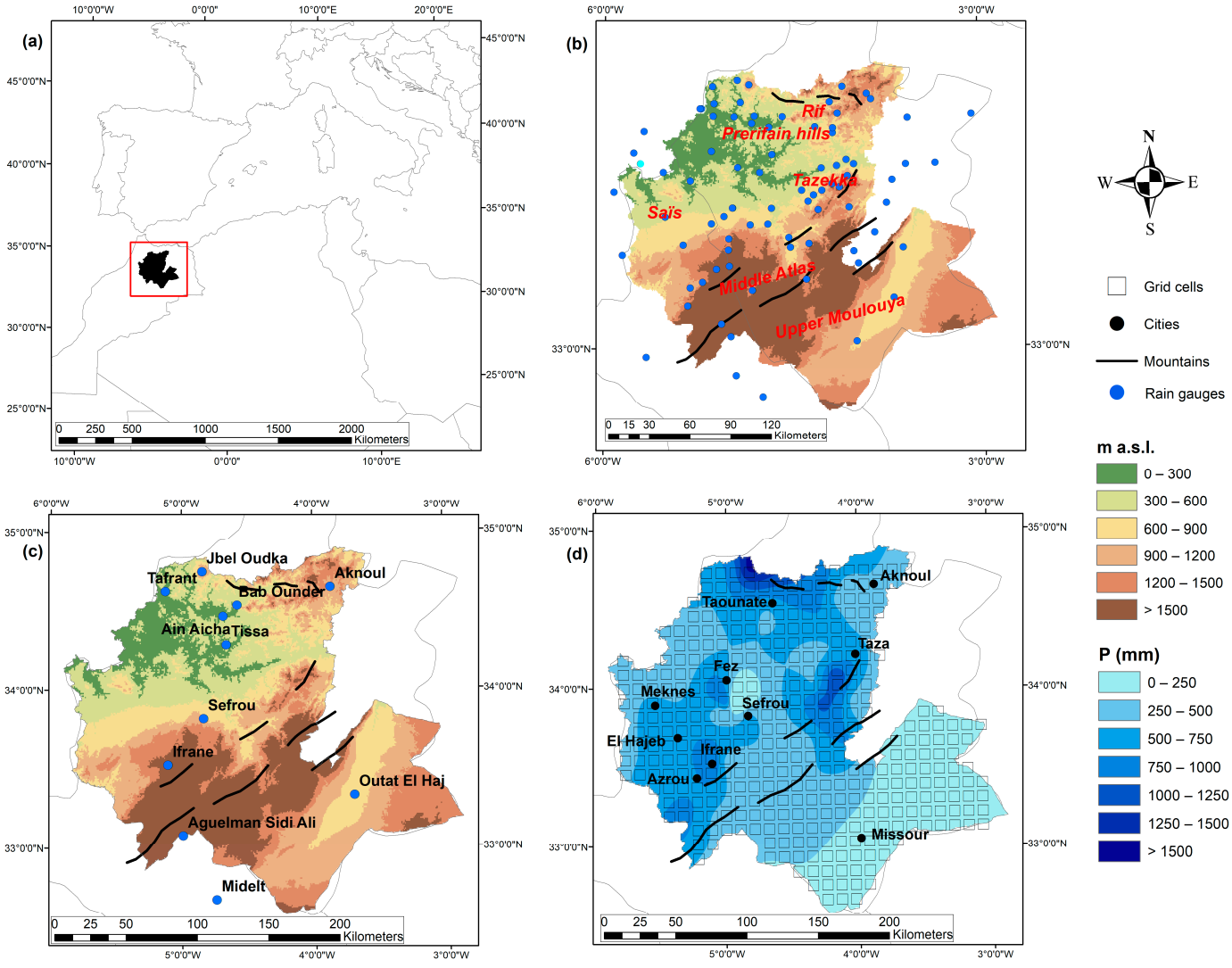


Figure 1. (**a**) localization of the study area (red box); (**b**) topography and rain gauge stations; (**c**) topography and rain gauge stations used for the wavelet analysis; (**d**) grid points, interpolated precipitation, and main cities. Black lines in (**b**–**d**) represent the main ridges of mountains.

3. Materials and Methods

3.1. Data Acquisition and Preprocessing

The gridded data used in this study derive from 83 stations with monthly resolution (blue points in Figure 1b) collected from different sources, mainly the hydrological agencies Agence du Bassin Hydraulique du Sebou (ABHS), Agence du Bassin Hydraulique de la Moulouya (ABHM) and the Direction de la Météorologie Nationale (DMN). This dataset was presented in detail in Kessabi et al. [35]. The station data were gridded through interpolation to 389 grid points, with 0.1° × 0.1° resolution (Figure 1c).

The inverse distance weighting (IDW) technique has been used to interpolate observed monthly data. A limitation of the IDW interpolation is that it relies primarily on spatial distance and does not explicitly incorporate physiographic factors such as elevation, slope, aspect, or exposure. In a topographically complex region such as Fez-Meknes, this may smooth local precipitation gradients and underrepresent sharp orographic contrasts, especially across the Rif and the Middle Atlas mountain sectors, and rain-shadow areas. Nevertheless, the interpolation procedure adopted here was previously evaluated using the available station network and provides a consistent spatial framework for the regional-scale analyses performed in this study. Specifically, these processing steps were presented and evaluated in detail in an earlier publication [36] together with the limitations and drawbacks of the method itself. This gridded dataset of monthly precipitation amounts was used to create seasonal totals used for correlation with climate indices in this paper.

Climatic indices were downloaded from institutional entities. The NAO index calculation of Jones et al. [37] has been chosen, with Reykjavik in Iceland and Gibraltar as reference points. In particular, the data on the NAO index used in this work are those of the CRU climate research unit at the University of East Anglia in England, available at the following link: https://crudata.uea.ac.uk/cru/data/nao/ (accessed on 31 October 2024). The East Atlantic (EA) pattern considered here is a prominent mode of low-frequency atmospheric variability in the 500-hPa geopotential-height field over the North Atlantic. The Climate Prediction Center (CPC) and the United States National Oceanic and Atmospheric Administration (NOAA) EA index used in this study is derived from standardized monthly 500-hPa geopotential-height anomalies using a rotated principal component analysis, following the methodology of Barnston and Livezey [21]. The data were obtained at the following link: https://ftp.cpc.ncep.noaa.gov/wd52dg/data/indices/ea_index.tim (accessed on 31 October 2024). The WeMO climate index data have been downloaded from the official website of the Climate Research Unit of the University of East Anglia at the following link: https://crudata.uea.ac.uk/cru/data/moi/Web_WeMOi-2020.txt (accessed on 31 October 2024). All the indices are in monthly resolution, and the data have been averaged to obtain seasonal values as follows: September, October, November = autumn; December, January, February = winter; March, April, May = spring; and June, July, August = summer. Although the NAO, EAP, and WeMO indices are based on different formulations, in this paper their established reference definitions have been retained to ensure consistency with the respective literature. The indices are therefore analyzed separately as diagnostics of distinct circulation patterns, and are not treated as directly commensurable measures of atmospheric variability.

3.2. Methods

The relationship between teleconnection indices and precipitation was explored using the Pearson correlation coefficient. Statistical significance was assessed through the p-value associated with each correlation coefficient. The symbol α denotes the predefined significance level, i.e., the threshold against which the p-value is compared. In this study, significance levels of $\alpha = 0.10$, 0.05, and 0.01 were adopted, and correlations were consid-

ered statistically significant when $p < \alpha$. The Pearson correlation coefficient was calculated as follows:

$$r = \frac{\sum_{i=1}^{n}(x_i - \overline{x})(y_i - \overline{y})}{\sqrt{\sum_{i=1}^{n}(x_i - \overline{x})^2}\sqrt{\sum_{i=1}^{n}(y_i - \overline{y})^2}}, \quad (1)$$

where r is the Pearson correlation coefficient, x_i and y_i are the individual paired values of the two variables, $\overline{x}$ and $\overline{y}$ are their respective arithmetic means, and n is the number of paired observations in the two time series. In this case, x and y are the time series of seasonal rainfall and seasonal values of the climate indices like NAO, EAP and WeMO. The R METAN (Multi-Environment Trial Analysis) package version 1.18.0 has been used [38]. This library was used to calculate the correlation coefficient and its associated p-value. Subsequently, correlations satisfying the predefined significance levels of $\alpha = 0.10$, 0.05, and 0.01 were mapped. To investigate interannual patterns in monthly rainfall in relation to the different phases of each climatic index, the months in the time series from the selected stations were classified according to the corresponding climate index phase $(-/+)$. Monthly precipitation probability density functions (PDFs) were then estimated using the normal (Gaussian) distribution.

The formula for the PDF is:

$$f(x) = \frac{1}{\sqrt{2\pi\sigma^2}} e^{\frac{-(x-\mu)^2}{2\sigma^2}}, \quad (2)$$

where x is the precipitation value, μ s the expected value (mean) of the normal distribution, σ is the standard deviation, and σ^2 is its variance [39].

Wavelet Transform (WT) is one of the most robust mathematical tools for analyzing non-stationary time series. The WT of a signal is its expansion using local basis functions, or wavelets, by dilation and translation. The WT decomposes the time series into time-frequency space to determine both the dominant modes of variability and how those modes vary in time [40]. The WT of a time series xt, is defined as [41]:

$$W_x(\tau, s) = \frac{1}{\sqrt{s}} \int_{-\infty}^{+\infty} x(t)\psi^*\left(\frac{t-\tau}{s}\right)dt, \quad (3)$$

where ψ* (t) is complex conjugate of "mother" wavelet ψ (t). The τ and s are translation and scale parameters, respectively. The "daughter" wavelets are obtained by translating and scaling the "mother" wavelet and are defined as:

$$\psi_{\tau,s}(t) = \frac{1}{\sqrt{s}}\psi\left(\frac{t-\tau}{s}\right), \quad (4)$$

The wavelet function chosen for this study is the Morlet wavelet. The Morlet wavelet is one of the most popular complex wavelet functions broadly used in geophysical and hydro-climatological studies, and is defined as follows [42]:

$$\psi_0(t) = \pi^{-1/4} e^{i\omega_0 t} e^{-t^2/2}, \quad (5)$$

where $\acute{\omega}_0$ is the dimensionless frequency which was chosen equal to 6 to satisfy the admissibility condition. The wavelet power spectrum is calculated as follows [43]:

$$\text{Power}(\tau, s) = \frac{1}{s}\left|W(s, \tau)\right|^2, \quad (6)$$

The cross wavelet transform of the two time series x_t and y_t is obtained from the relation with the WT of W_x and W_y as follows [43,44]:

$$W_{xy}(\tau, s) = \frac{1}{s} \cdot W_x(\tau, s) \cdot W_y(\tau, s), \quad (7)$$

Cross wavelet power is the modulus of cross wavelet transform and is obtained from the following equation [45]:

$$Power_{xy}(\tau, s) = \left|W_{xy}(\tau, s)\right|, \quad (8)$$

The cross-wavelet transform can lead to misleading results because it is not normalized. The Wavelet Coherence (WC) solves this problem by normalizing to the single wavelet power spectrum. The WC between two time series x and y is given by [46]:

$$WC = \frac{\left|S.W_{xy}(\tau, s)\right|^2}{S.\text{Power}_x \times \text{S.Power}_y}, \quad (9)$$

where S is a smoothing operator.

Wavelet coherence was computed using the complex Morlet wavelet with $\omega_0 = 6$. The coherence between the two time series was obtained from the smoothed cross-wavelet spectrum normalized by the corresponding smoothed individual wavelet power spectra, as expressed in Equation (9), where S denotes the smoothing opùerator applied in both time and scale. Statistical significance of the wavelet coherence was assessed at $\alpha = 0.05$. The significance levels calculated for individual grid cells should be interpreted as local, nominal significance levels. Because the 389 precipitation series were obtained by spatial interpolation from 83 stations, neighboring grid cells are spatially correlated and therefore do not constitute independent statistical tests. Spatial dependence was therefore additionally evaluated using a permutation-based procedure. To preserve the spatial covariance structure of the precipitation field, the temporal permutation was applied identically to all grid cells rather than independently at each location. Spatial autocorrelation of the resulting patterns was quantified using Moran's I and compared with the distribution obtained from common-year permutations. The effective number of spatially independent tests was also estimated from the covariance structure of the gridded precipitation field. The effective number of spatially independent tests was additionally estimated from the covariance structure of the gridded precipitation field. Accordingly, the percentages of locally significant grid cells reported below are used primarily to describe the spatial extent and coherence of the teleconnection–precipitation relationships, rather than as counts of statistically independent significant locations.

4. Results

4.1. Association Between the NAO and Seasonal Precipitation

The results of the correlation between seasonal rainfall and the NAO index for all 389 grid points covering the Fez-Meknes region are presented in Figure 2.

Winter and autumn exhibited a spatially coherent negative relationship with the NAO across virtually the entire interpolated precipitation field. In fact, for $\alpha = 0.01$, 99.7% and 97.4% of grid cells showed significant correlations for winter and autumn, respectively. Because neighboring grid cells are spatially dependent as a consequence of both the intrinsic spatial coherence of precipitation and the interpolation procedure, these percentages are used here as a descriptive measure of spatial coverage rather than as the proportion of independent significant observations. This spatially coherent relationship indicates a strong association between the NAO and rainfall conditions within the study area during both seasons. The spatial dependence analysis confirmed that the grid cells cannot be regarded as independent observations. For example, Moran's I for the spatial pattern was approximately 0.80. Although a conventional Moran test assuming spatial independence would indicate highly significant clustering ($p < 0.001$), the common-year permutation test, which preserves the covariance structure of the precipitation field, yielded $p = 0.24$. Thus, the observed

spatial clustering does not exceed that expected from the strong regional covariance of precipitation. Consistently, the effective number of independent spatial tests was estimated at approximately 1.1, indicating that the 389 interpolated grid cells essentially represent one dominant regional spatial signal. On the other hand, the correlation between spring rainfall and the NAO becomes less strong, with 77% of grid points meeting the nominal local significance thresholds, with 32.6% of cells at the 10% significance level, 40.1% at the 5% level, and only 4.4% at the 99% confidence level. On the other hand, 23% of the points record a non-significant correlation with the NAO index of the same season (Figure 2). In summer, when precipitation is already low, the correlation coefficient becomes insignificant on 98.2% of the grid points. Only 7 points, or 1.8% of the total, record a nominally significant correlation at the threshold of $\alpha = 0.1$.

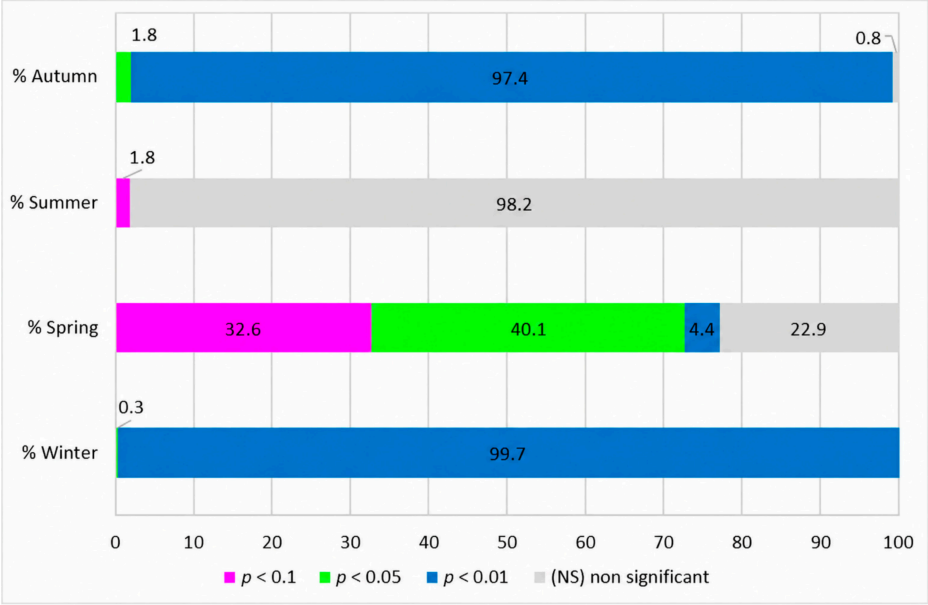


Figure 2. Percentage of grid points having a significant correlation between seasonal rainfall and NAO at thresholds 0.1, 0.05 and 0.01 (NS: non-significant correlation).

At the spatial level, the two seasons of autumn and winter record the strongest and most significant negative correlations over practically the entire territory of the Fez-Meknes region (Figure 3). In winter, the correlation coefficient ranges from −0.45 to −0.84, and 379 out of 389 grid points recorded a more negative coefficient equal to −0.70 or less, representing 97% of the grid points distributed evenly over the entire study area. The same pattern has also been detected in the relationship between autumn rainfall and the NAO index, with 379 points recording a significant negative correlation at the 99% threshold, with a correlation coefficient oscillating between −0.34 and −0.57 (Figure 3). Only 7 points showed correlations significant at the 5% threshold, and 3 points recorded a non-significant correlation. In general, autumn and winter do not present any distinct spatial mode because of the relief or the exposure; the response of the rainfall of the two seasons to the NAO patterns is almost the same over the entire regional territory. As regards the correlation between spring rainfall and the spring NAO index, in the north of the study area, 14 points showed a significant correlation at the significance level of $\alpha = 0.01$ (Figure 3). They are concentrated around Taounate and Jbel Oudka; the correlation coefficient of this sub-region varies between −0.34 and −0.38. The rest of the northern half of the study area reveals a significant correlation with $\alpha = 0.05$, and the correlation coefficient varies between −0.24 and −0.33. The southern half of the region records significant correlations with $\alpha = 0.1$ (Figure 3), with several non-significant cells, especially beyond the Middle Atlas ridges

and the upper Moulouya. In summer, an almost total absence of significant correlations emerged in the study area, except for a few cells on mountain peaks, which can be linked to convective storm showers.

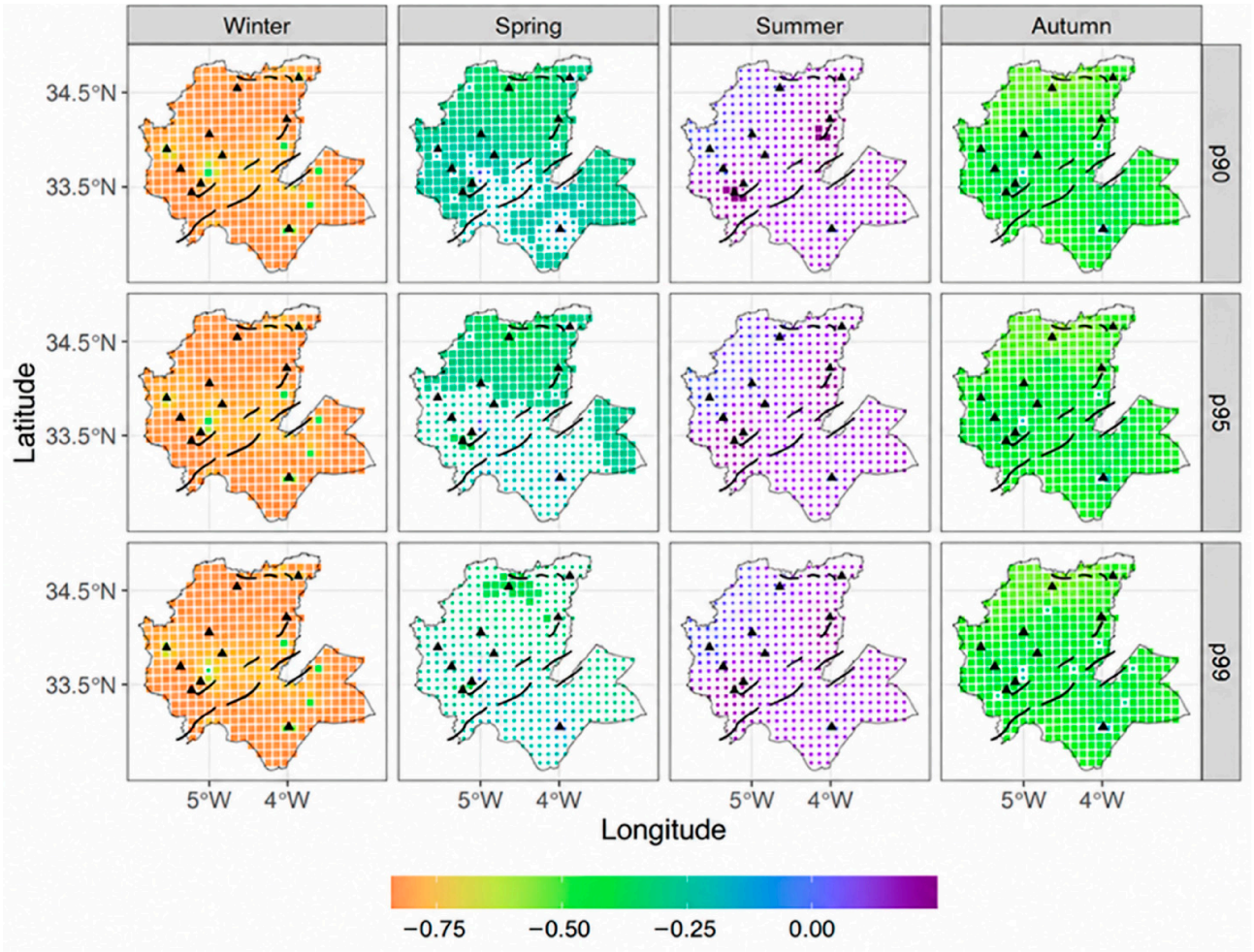


Figure 3. Correlation coefficient by grid points between rainfall and NAO of the four seasons (Square dimensions indicate the significance level of the correlations: large squares: significant correlation, small squares otherwise; colors show values of CC).

Figure 4 shows the PDF of the monthly rainfall data from the Ifrane station according to the two phases of the NAO index. It turns out that rainfall associated with months with a negative NAO index, represented by the blue curve, is greater in frequency and quantity above the 125 mm level. At the same time, the black curve reflects the relatively high frequency of months associated with an NAO+ index with rainfall values less than 125 mm. The fact that NAO+ events have been more frequent during the last four decades helps to explain the frequent droughts the study area experienced.

In order to carry out a more in-depth analysis of the NAO on the increase or decrease in rainfall during the seasons most correlated with this index (winter, autumn and spring), the percentage of change between the average precipitation during the two phases of the NAO index has been calculated. Then, these values have been compared with the average of the two seasons during the whole period studied, 1961–2019 (Figure 5).

During winter, the positive phase of the NAO is associated with precipitation amounts 30–37% below the long-term seasonal average in the wettest areas of the Western Rif and the Middle Atlas Mountains close to Ifrane (Figure 5). A smaller reduction between 14% and 26% is recorded between Sefrou and Missour, with a pronounced shelter effect. The rest of the

region's territory, especially between Meknes and Taza, shows reduction rates of 26% to 30%. As an example, during winter 1994/95, the region experienced a domination of the positive phase of the NAO (Figure 6A) and recorded only 58 mm as a regional winter average, which deviates significantly from the regional normal of 196 mm. On the other hand, the negative phase of the NAO is associated with higher precipitation amounts over the entire study area. Increase rates between 44% and 57% are recorded in the north and the southwest of the region. Between Meknes and Taza, the increase rates are between 40% and 44% compared to the seasonal average. The gray areas between Sefrou and Missour record a 20% to 40% rainfall surplus linked to the NAO compared to the seasonal normal (Figure 5). These results indicate a very strong association between the NAO and winter rainfall within the study area. For example, during the wet year 2009/2010, with a negative NAO index of −3.34, the region accumulated a record winter rainfall of 504 mm. The atmospheric situation was marked by a clearly negative anomaly of atmospheric pressure over the mid-latitudes and a positive one over the Arctic (Figure 6B). In autumn, the positive phase of the NAO is characterized by a clear reduction in rainfall, between 20% and 32%, in the north and northwest. Between Sefrou and Missour, the reduction rate is 13% to 17%. The rest of the region's territory records reductions of between 17% and 20%. Furthermore, autumn rainfall shows a stronger association with the positive phase of the NAO index than with its negative phase; the decreases in precipitation during positive episodes of this index are very large compared to the increases in precipitation during negative phases (Figure 5).

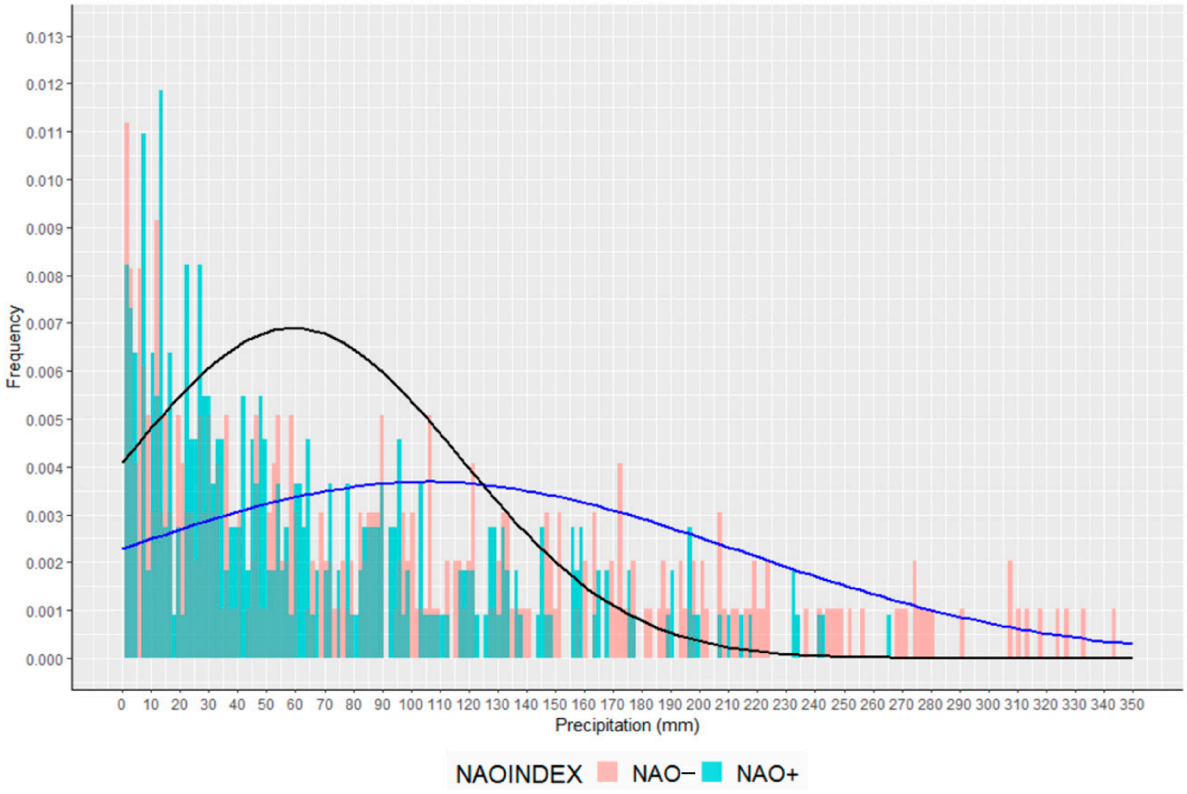


Figure 4. Histogram and smoothed probability density function for monthly rainfall data from the Ifrane station according to the two phases of the NAO index (the blue line NAO−, the black line NAO+).

In spring, the positive phases of the NAO are accompanied by a rainfall anomaly of between −7% and −12% compared to the average of the period (1961/2019) over the northern half of the region, and between −4% and −7% over the rest of the region's territory. On the other hand, the negative phases of the NAO present an increase in rainfall between +9% and +17% in the northern half of the region (Figure 5). Over the observation period (1961–2019),

there were 42 autumn seasons with a NAO− index and only 17 seasons with a NAO+ index, which provides clarification on the non-significant increase in autumn rainfall mentioned by past studies such as those of Kessabi et al. [47] and Addou et al. [48]. Moreover, the observation period included 35 winter seasons with a NAO+ index and only 23 seasons with a NAO− index. This is consistent with the observed decrease in winter precipitation over the study area in this period, at least partly linked to the persistence of the NAO+, which has been reported and confirmed in past works such as those of Knippertz et al. [15], Born et al. [49], Kessabi et al. [36] and Kessabi et al. [50].

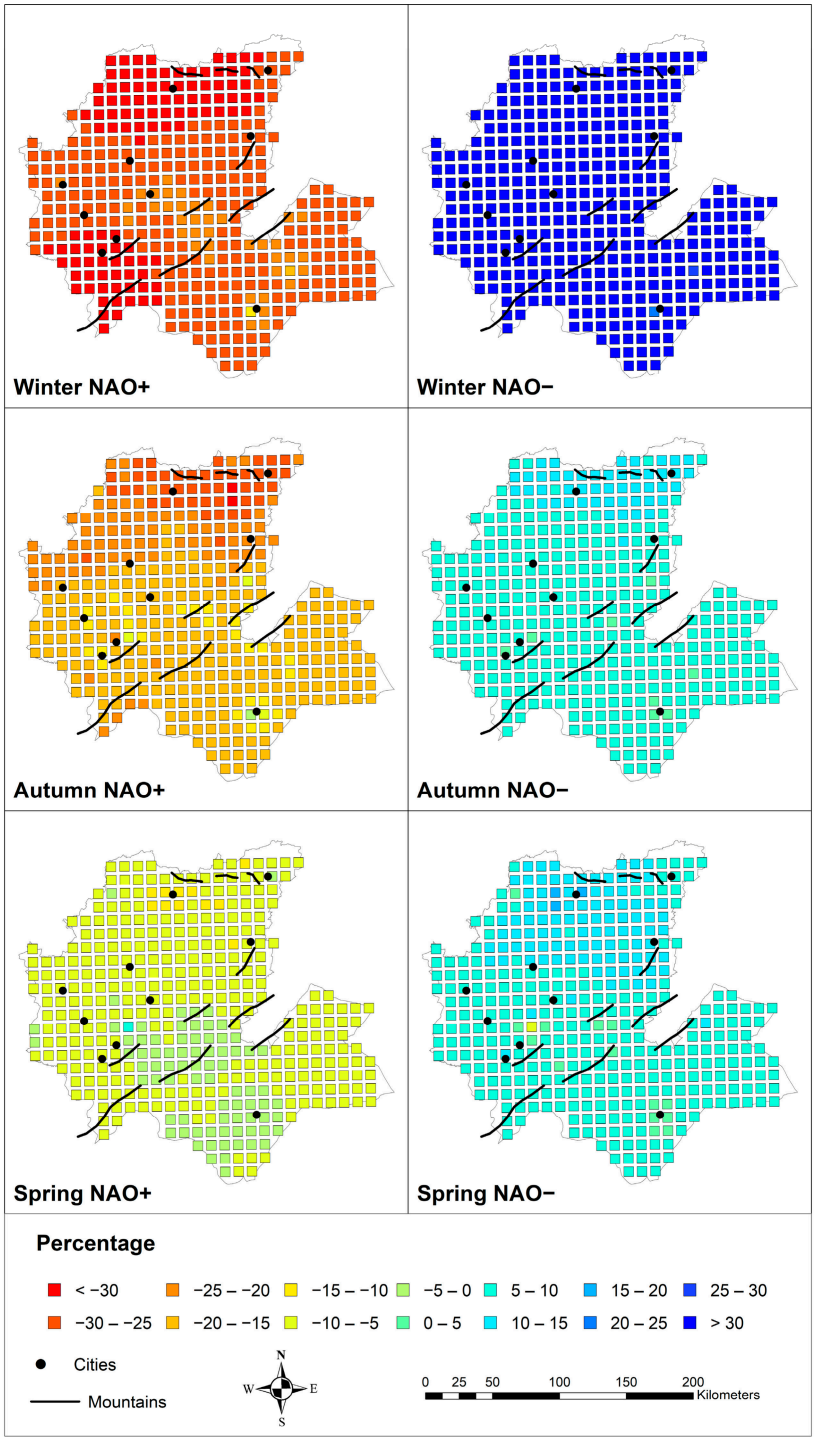


Figure 5. Percentage increase or reduction in precipitation relative to the long-term average according to the two phases of the NAO index for winter, autumn and spring.

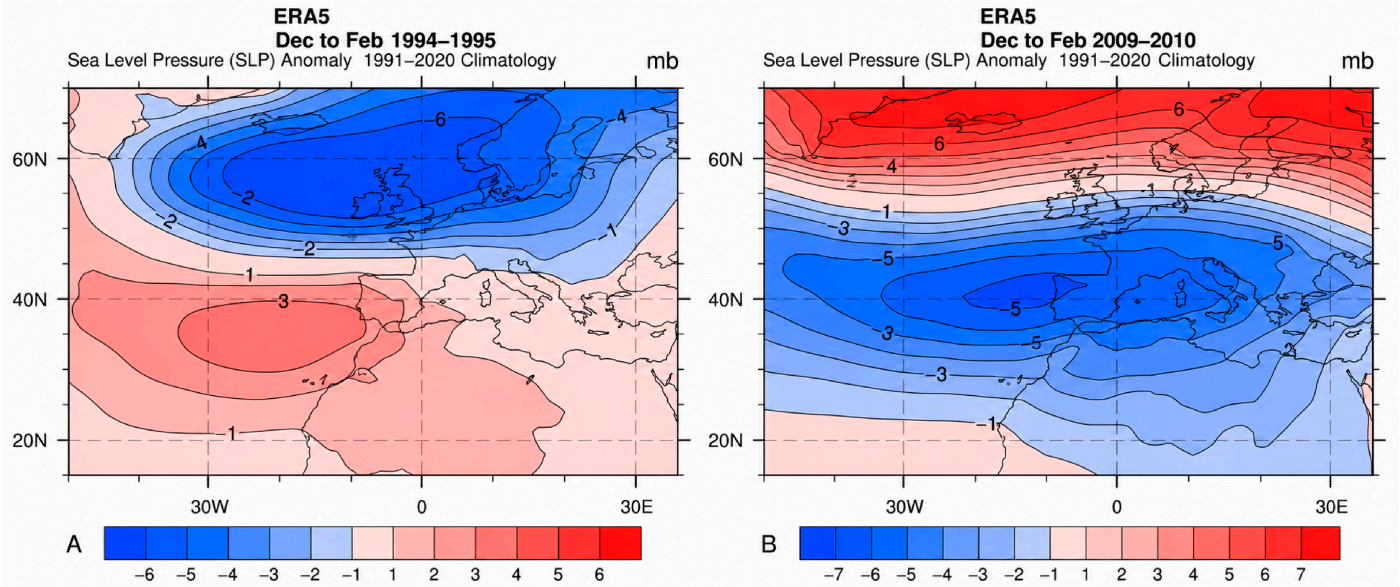


Figure 6. Anomalies of atmospheric pressure at sea level in winter during a positive phase of the NAO in the winter of 1994–1995 (**A**) and a negative phase of the NAO in the winter of 2009–2010 (**B**) (Data source: https://psl.noaa.gov/data/getpage/, accessed on 26 October 2026).

4.2. Association Between the EAP and Spring Precipitation

The results of the correlations with the East Atlantic Pattern index (EAP) are presented in Figure 7 as a percentage of the grid points and according to the level of significance of the correlation. Spring rainfall shows the strongest association with this index. Based on the local nominal tests, 95% of the grid cells have negative correlations with $p < 0.01$, while a further 4.4% have $p < 0.05$. Because of the strong spatial dependence demonstrated by the permutation analysis, these percentages should be interpreted as measures of the spatial extent and coherence of the EAP− precipitation relationship rather than as proportions of independent significant tests. Summer precipitation shows weaker associations: 22% of grid cells have nominal $p < 0.1$, 15.7% have $p < 0.05$, and 2.3% have $p < 0.01$, whereas approximately 60% show no nominally significant correlation. The other two seasons (autumn and winter) do not present any significant correlation over the entire study area; the correlation coefficients remain very low.

Unlike the winter and autumn seasons, spring precipitation shows stronger correlations with the EAP index. Significant correlations at the 0.01 threshold are distributed homogeneously over the entire territory of the region (Figures 8 and 9). The northwestern tip of the region, which recorded correlations only significant at the 0.05 threshold, represents an exception in this regard. The correlation coefficient varies between −0.34 and −0.51 for the group of cells with significant correlations at the 0.01 threshold, and between −0.28 and −0.33 for points which recorded significant correlations with $\alpha = 0.05$. Despite the fairly low level of summer precipitation and their convective or even non-homogeneous characters with an absence of a general mode which governs them, summer comes in second position in terms of correlations with the EAP index; the correlations remain weakly significant at the thresholds 0.1 and 0.05 in the northern half of the study area (Figure 8).

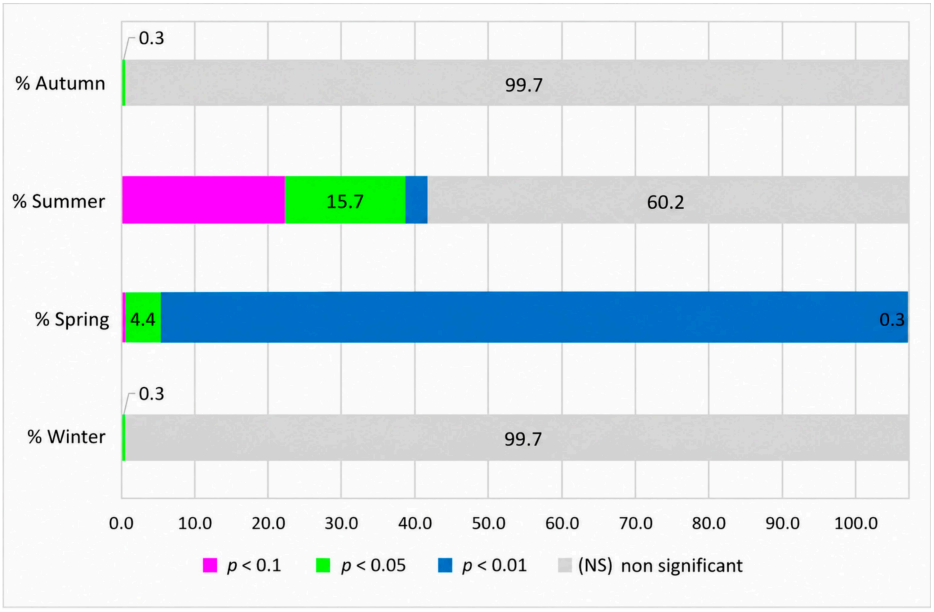


Figure 7. Percentage of grid points with a significant correlation between seasonal rainfall and EA oscillation at thresholds 0.1, 0.05 and 0.01 (NS: non-significant correlation).

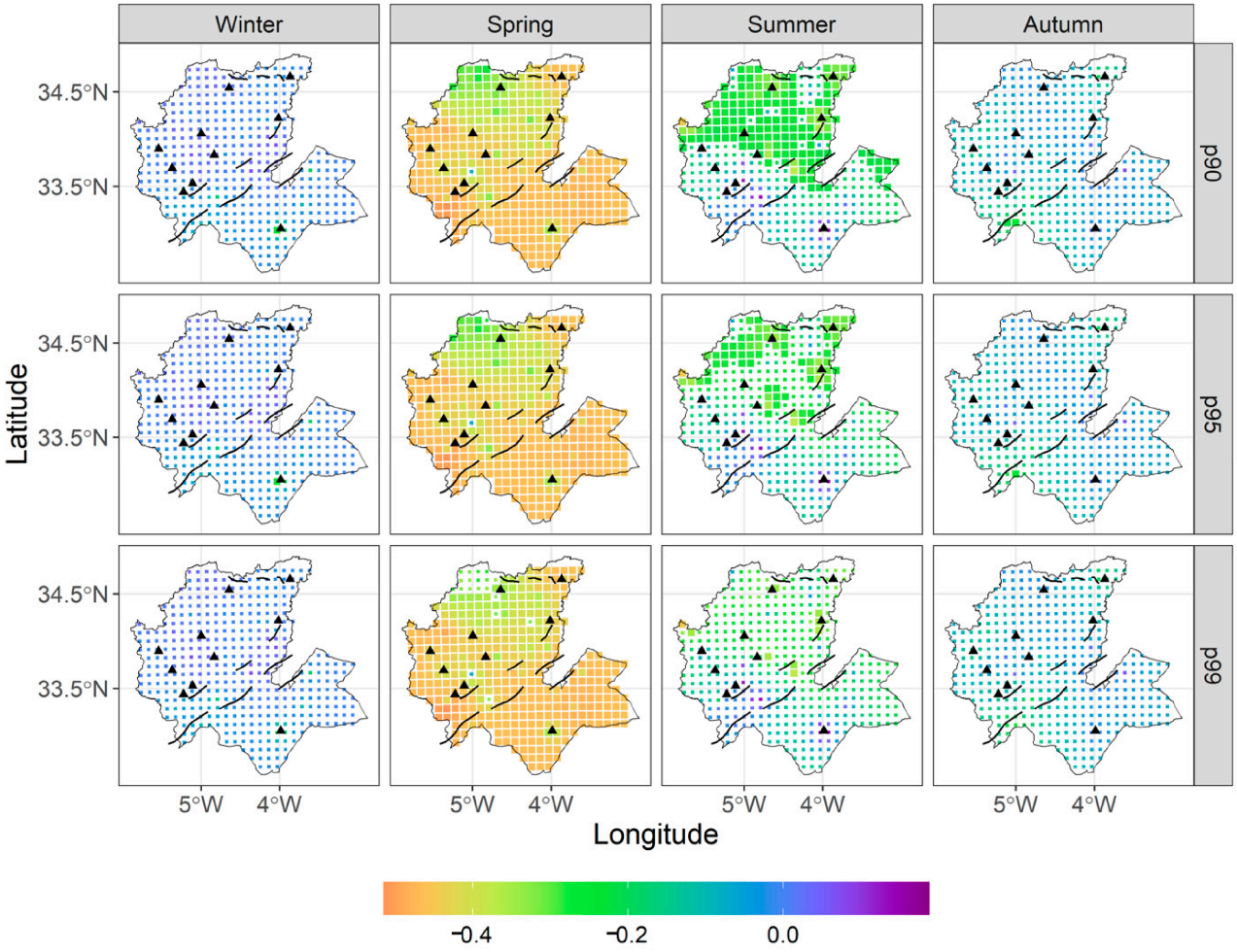


Figure 8. The correlation coefficient between rainfall of the four seasons and EAP index. (Square dimensions indicate the significance of the correlations: large squares: significant correlation, small squares otherwise).

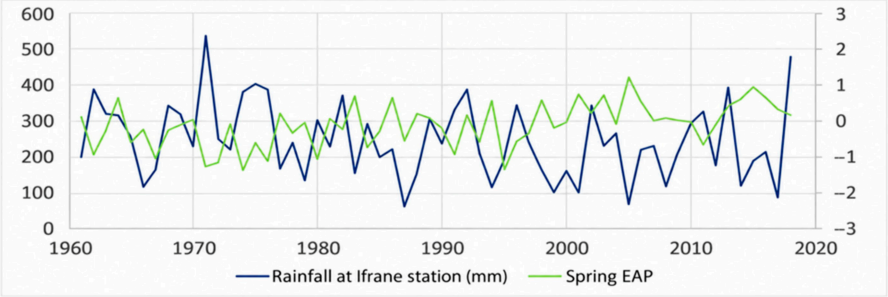


Figure 9. Interannual variability of spring rainfall at Ifrane station and the EAP index of the same season during the period 1961–2019. (The negative correlation between the two series is significant at the threshold $\alpha = 0.01$).

The areas extending westward from Taounate, as well as the eastern part of the region, between Taza and Aknoul, present significant correlations at the 0.05 threshold. This provides new explanations for the first time for summer precipitation in our study area. The correlation coefficients oscillate between −0.22 and −0.31 for the 85 points correlated at the threshold 0.1, and between −0.24 and −0.33 for the group of points correlated at the threshold 0.05. The nine points which record a correlation at the 0.01 threshold have correlation coefficients between −0.34 and −0.38 (Figure 8). The relationship between the EA index and summer rainfall is therefore concentrated on the northern half of the region, while the southern half of the region only records non-significant correlations. The relief of the region, represented by the ridgelines in the previous maps, appears to have no influence on the correlations with the EAP index. Instead, the latitudes and the distance from the sea might affect the relationship between the EAP index and the spring or summer rainfall in the region. By applying the PDF to all monthly data from the Sefrou station, Figure 10 evidences that months with a negative EAP index are more likely to record moderate to heavy precipitation (60–200 mm, the blue line) compared to months that correspond to a positive EAP index (the pink line).

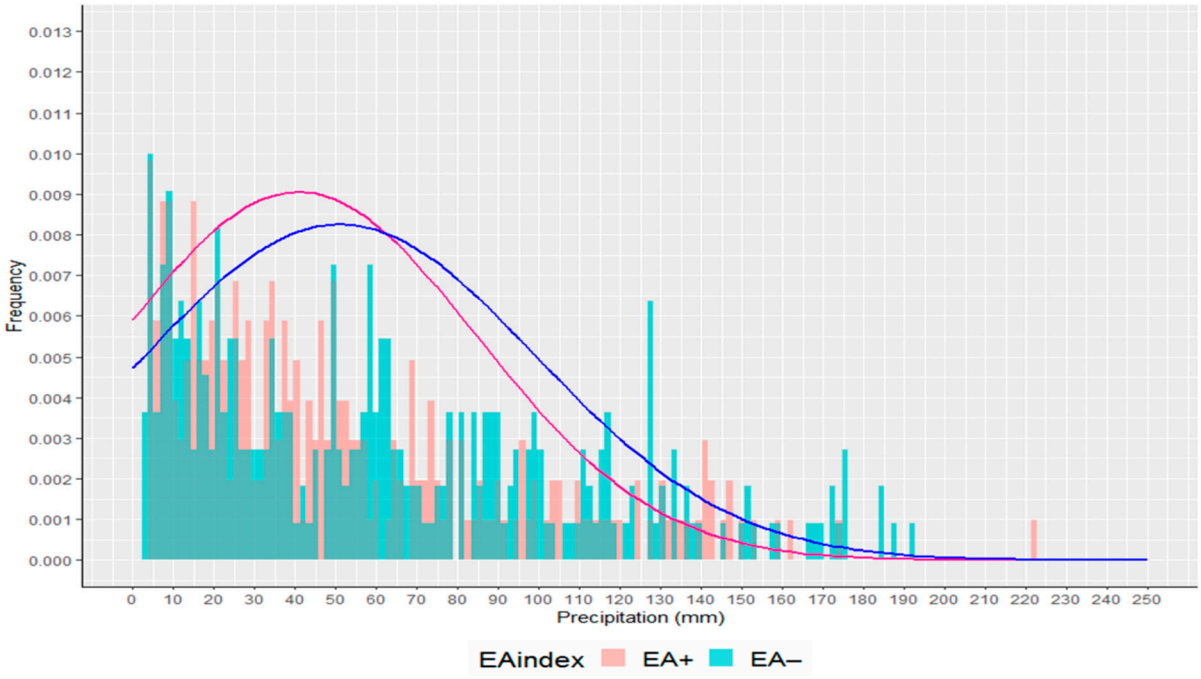


Figure 10. Histogram and smoothed probability density function for monthly rainfall data from the Sefrou station (S65) according to the two phases of the EAP index (the blue line EAP−, the pink line EAP+).

The precipitation anomalies associated with the EAP are quantified via the difference in means between the negative and positive phases of this index and in relation to the average of the period studied (1961–2019). Positive EAP phases are associated with a very strong reduction in spring precipitation in the arid to semi-arid regions of Moulouya, which reaches up to −33%, and between −12% and −15% in the humid regions. The northwest tip of the region records the smallest reductions, between −11% and −1% (Figure 11).

During positive EAP phases, precipitation was lower than the long-term average in the High Plateau of Moulouya, which is known for a dominant spring rainfall regime [51–53]. The share of spring precipitation in the total annual precipitation can reach 40% in Outat El Haj and 39% in Missour. The excess precipitation during the negative phases of this EAP index varies between 14% and 24% compared to the average of the period 1961–2019, which does not allow the reduction during the positive phases of the EAP index to be compensated. Similarly to the NAO, this index shows an increasing trend towards its positive phases, thus contributing to a decrease in spring precipitation in the arid regions of Moulouya [54].

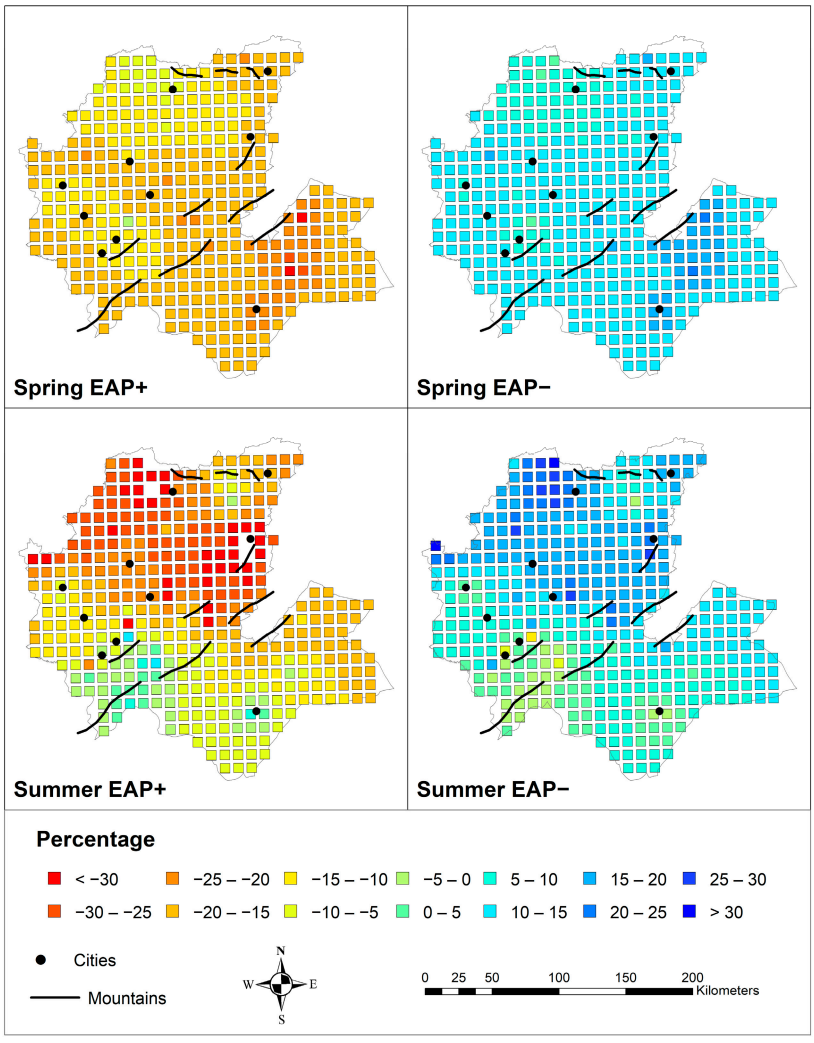


Figure 11. Percentage (%) of change in average spring and summer precipitation according to the EAP+ and EAP− index.

Two typical cases of this EAP effect are the spring of 1977 for an EAP+ index and that of 1971 for an EAP− index (Figure 12). In the first case, the total rainfall amount recorded was 89 mm, well below (−44%) the seasonal average for the period studied which is around 158 mm. On the other hand, the spring rainfall during the second case of 1971 reached

338 mm, corresponding to 114% more than the seasonal normal. At the atmospheric level, there was a very strong negative pressure anomaly, centered on the Iberian Peninsula and northern Morocco during the EAP− phase of 1971; the opposite has been observed during the EAP+ phase of 1977. Indeed, the spring of 1977 recorded a positive pressure anomaly on the Gulf of Cádiz exceeding 2 hPa (Figure 12A). In summer, precipitation is very low or even absent over a large part of the study area. However, the mountain areas record significant shares of summer rains, which represent an average between 10% and 17% of the annual total. The positive phase of the EAP is associated with the reduction of summer precipitation in the area between the Middle Atlas piedmont, the northern Middle Atlas, the Saïs, and the extreme northwest and northeast of the region. This reduction is between −13% and −47%. On the other hand, during the negative phase of the EAP index, the increase in rainfall varies between 8% and 37% on the northern half of the study area and between 2% and 8% on the northwest and southeast of the Middle Atlas range (Figure 11).

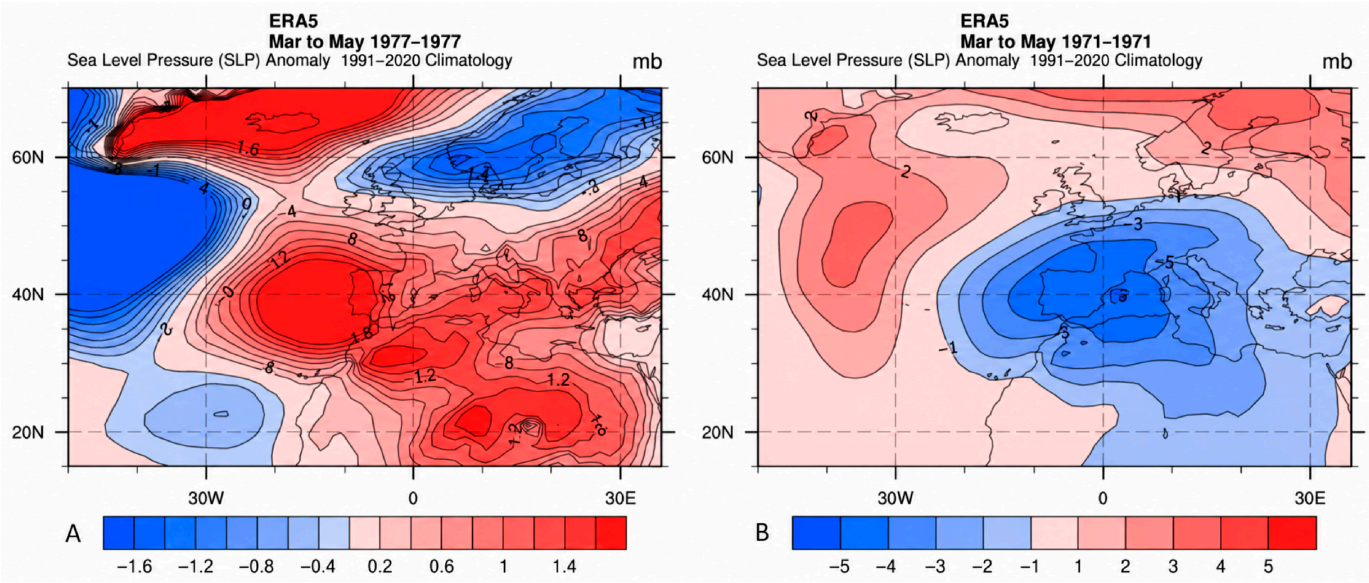


Figure 12. Anomalies of atmospheric pressure at sea level in spring during the positive phase of the EAP of the year 1977 (**A**) and the negative phase of the EAP of the year 1971 (**B**) (Data source: https://psl.noaa.gov/data/getpage/, accessed on 26 October 2026).

4.3. Association Between the WeMO and Autumn Precipitation

The result of the correlation between precipitation in the study area and the West Mediterranean Oscillation (WeMO) index is summarized in Figure 13. The northern half of the study area records no significant correlation between winter rainfall and the WeMO index. Autumn precipitation showed the strongest relationship with the WeMO. Based on the local nominal tests, 96.14% of the grid cells showed negative correlations with $p < 0.01$, with Pearson correlation coefficients ranging from −0.27 to −0.45; the remaining cells had $p < 0.05$, with correlation coefficients ranging from −0.10 to −0.21. As discussed above, because neighbouring grid cells are strongly spatially dependent, these percentages describe the spatial coherence of the WeMO− precipitation relationship and should not be interpreted as percentages of independent significant tests (Figure 14). Winter precipitation showed a weaker relationship with the WeMO: 44.2% of the grid points exhibited significant correlations at $\alpha = 0.01$, while 9.3% were significant at $\alpha = 0.05$ (Figure 13).

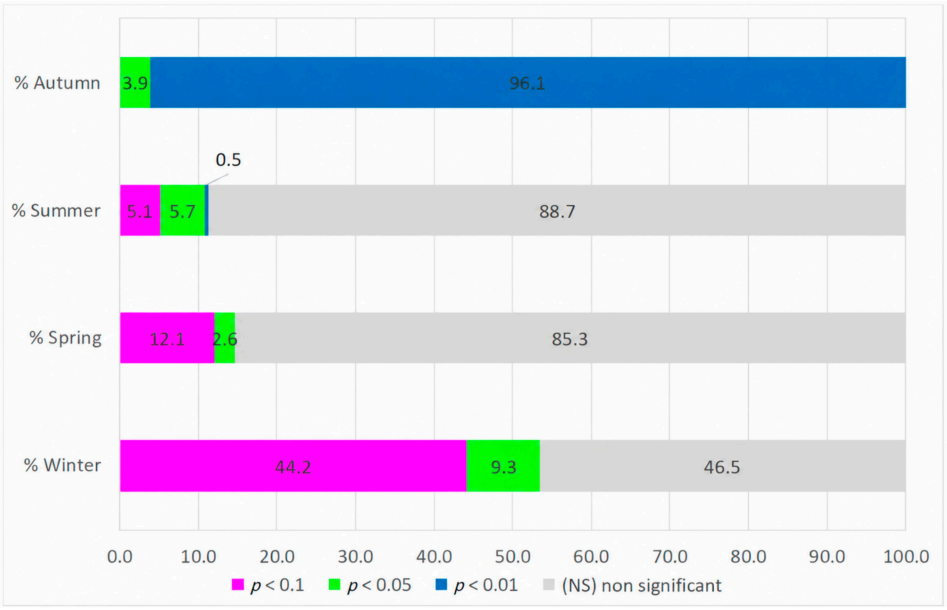


Figure 13. Percentage of grid points with a significant correlation between seasonal rainfall and WeMO oscillation at thresholds 0.1, 0.05 and 0.01 (NS: non-significant correlation).

The corresponding correlation coefficients ranged from −0.22 to −0.29 and from −0.26 to −0.29, respectively (Figure 14). For spring, 12% of the grid points showed significant correlations at $\alpha = 0.01$, while 2.6% were significant at $\alpha = 0.05$, with correlation coefficients ranging from −0.22 to −0.26 and from −0.26 to −0.32, respectively. The correlation coefficients vary between −0.22 and −0.26 for the first group and between −0.26 and −0.32 for the second group. The rest, i.e., 85% of grid points, show no significance with this climatic index. The correlations of the non-significant points vary between 0.10 and −0.22. The correlations between autumn precipitation and the WeMO show a spatially coherent pattern, with most grid points significant at $\alpha = 0.01$ across the Fez-Meknes region. In winter, the significant correlation mainly concerns the southern part of the study area.

In order to confirm these results, Figure 15 shows the smoothed probability distribution of monthly rainfall according to the two phases of the WeMOi index at the Ain Aicha station. The blue curve corresponds to the months with a negative WeMO− index, and the black curve corresponds to the months with a WeMO+ index. Small amounts of precipitation (<65 mm) resulted more frequent in months with a WeMO+ index, while classes of large amounts of precipitation (>65 mm) are linked to months with a WeMO− (Figure 15). This result confirmed the observations on the effect of WeMO, which is synonymous with the abundance of precipitation throughout the study area in autumn and partly in winter, in the southern part of the region. Given the importance of the WeMO for the autumn rains, the difference, in percentage, between the average of the autumn precipitations, during the WeMO+ and WeMO− phases, compared to the average of the period studied (1961–2019) and by grid point are calculated and presented in Figure 16. During the positive phases, precipitation was lower by 6.7% up to more than 17% compared to the autumn average of the period (1961–2019). On the contrary, during the negative phases of the WeMO index, autumn precipitation was higher by 6.9 than more than 17% compared to the normal of the same period studied.

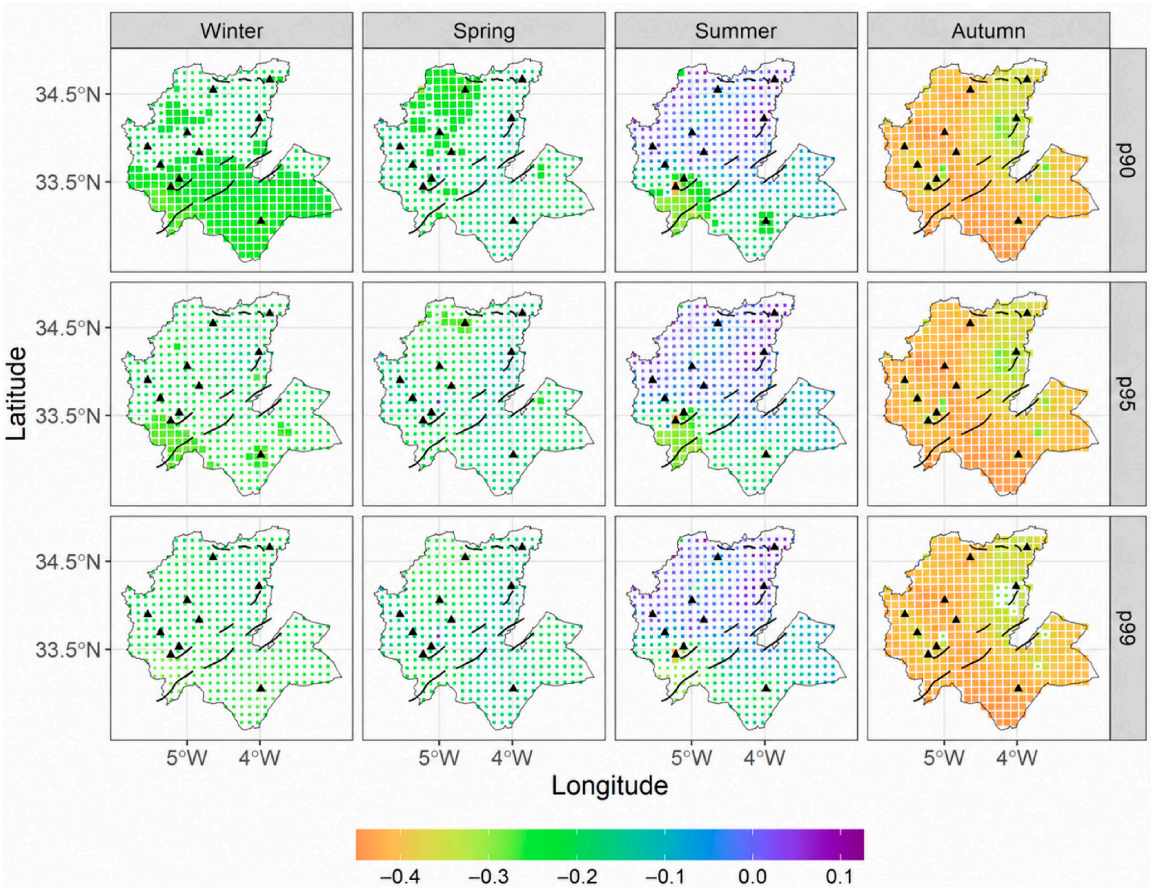


Figure 14. Correlation coefficient between seasonal rainfall and the WeMO index at each grid point. Colors indicate the values of the Pearson correlation coefficient, while square size indicates statistical significance: large squares denote significant correlations and small squares denote non-significant correlations.

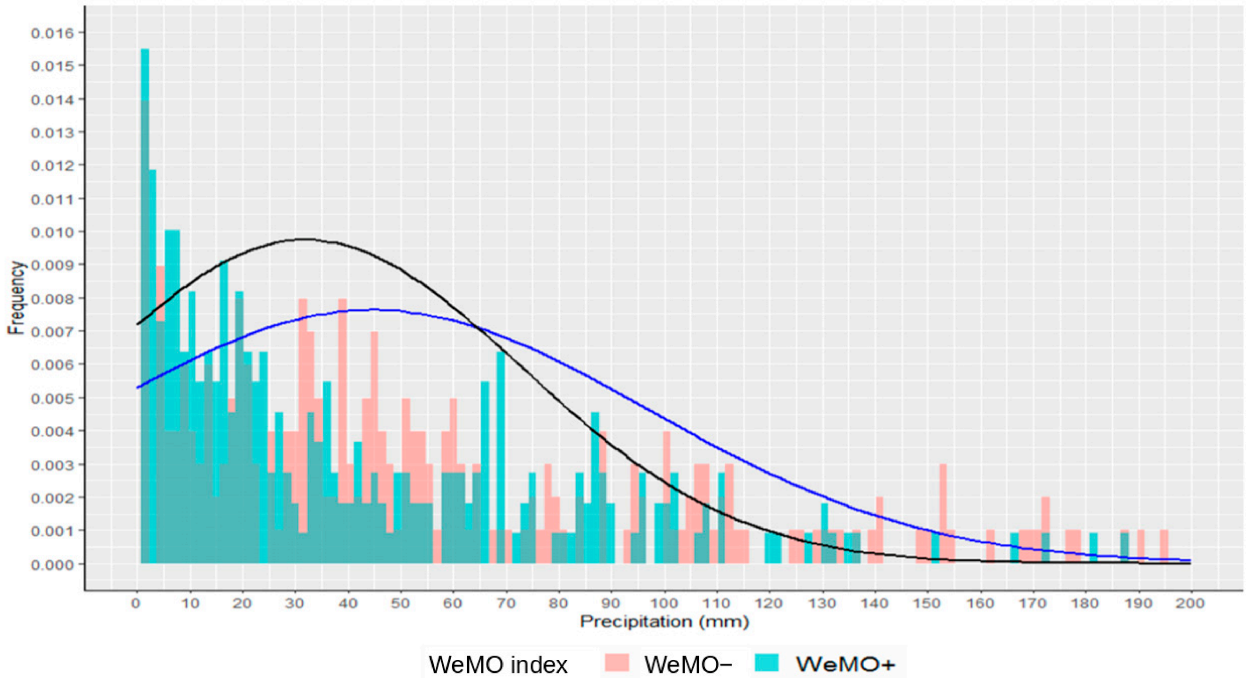


Figure 15. Histogram and smoothed PDF for monthly rainfall data from the Aïn Aïcha station according to the two phases of the WeMO index (the blue line WeMO−, the black line WeMO+).

Spatially, the Middle Atlas mountain areas recorded the least significant variations, between 7 and 9.5% more or less, in the WeMO− and WeMO+ phases. On the other hand, upper Moulouya and the northwest tip of the region recorded the maximum percentage variation, i.e., values between 13 and 17% more or less in the WeMO+ and WeMO− phases (Figure 16). The other zones recorded variations ranging from +/−11% to +/−13% depending on the WeMO−/+ phases.

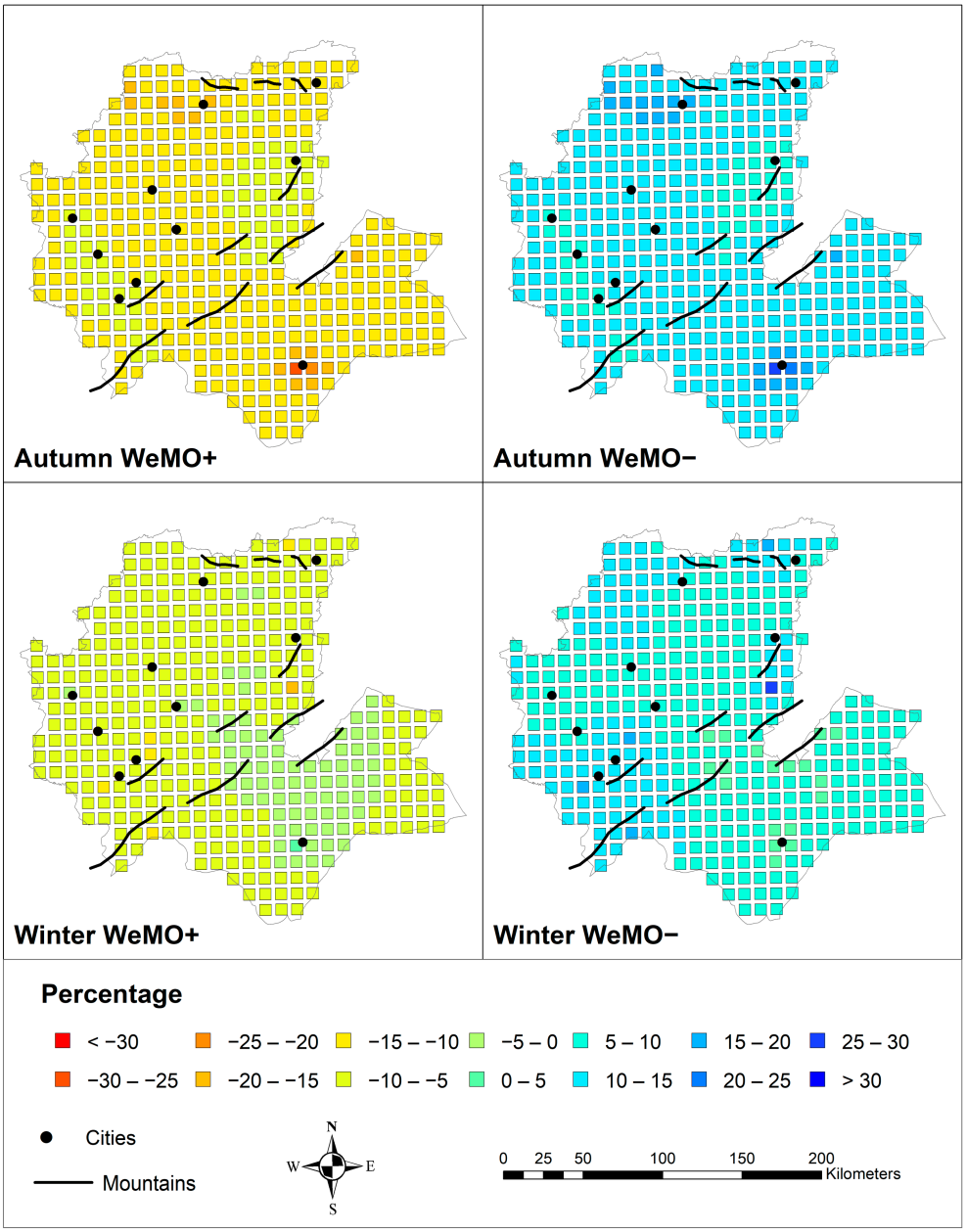


Figure 16. Percentage (%) of change in average autumn and winter precipitation according to the WeMO+ and WeMO− phases.

In winter, the relationship with the WeMO is evident in the Middle Atlas, the northeast and northwest tips of the Fez-Meknes region. The rates of increase during negative phases go from 10% to 26%, while the reduction is between 7% and 19% during positive phases of WeMO.

Figure 17 illustrates the atmospheric configurations according to sea level pressure anomalies in positive and negative WeMO phases. During the autumn of 1974, with a

WeMO+ index, the atmospheric situation generated only 49 mm of precipitation compared to a seasonal average of 134 mm. Otherwise, during the WeMO negative phase, the study area recorded a height of 175 mm of rain during the fall of 1989, which is higher than the seasonal normal.

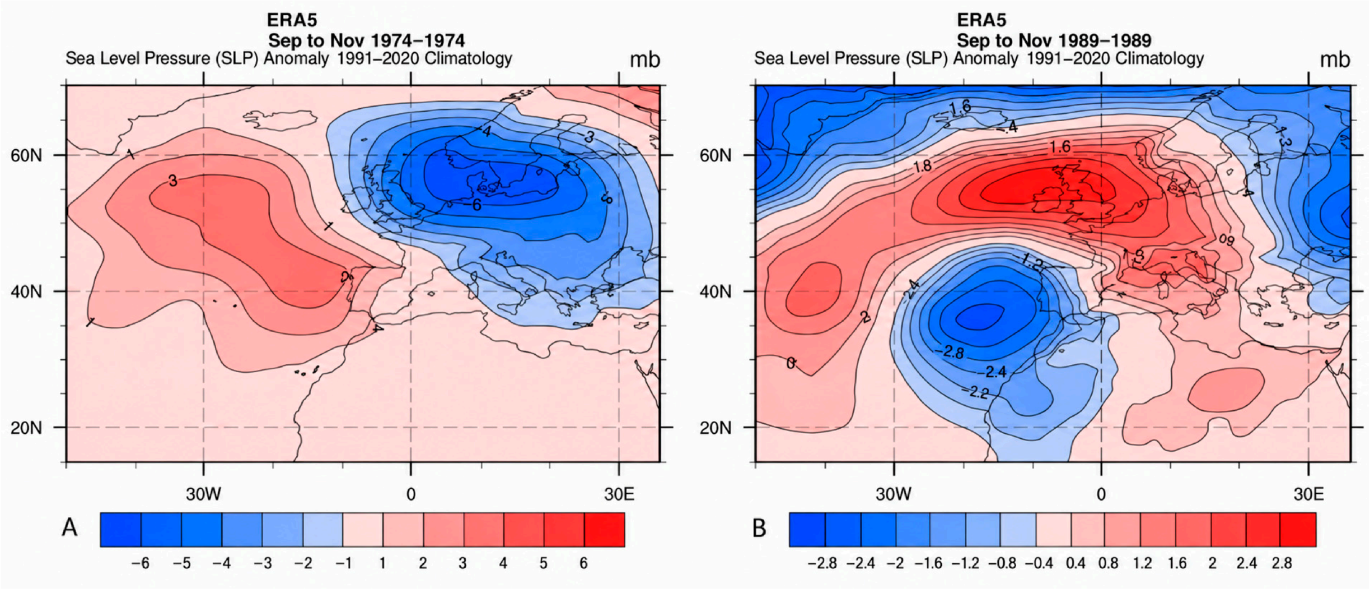


Figure 17. Anomalies of atmospheric pressure at sea level in autumn during the positive WeMO phase of the year 1974 (**A**) and the negative WeMO phase of the year 1989 (**B**) (Data source: https://psl.noaa.gov/data/getpage/, accessed on 26 October 2026).

4.4. Wavelet Coherence Analysis of Precipitation and Atmospheric Indices

The wavelet analysis has been performed considering selected stations able to represent contrasting hydroclimatic settings within the study area, including wetter northwestern and mountainous sectors and drier rain-shadow areas (Table 1 and Figures 18–20).

Table 1. Dominant periods and occurrence years for correlation with precipitation during 1961–2018 in the studied stations.

Climatic Indices	Stations	ID	The Periods of Variability in Years				
			1	**1–2**	**2–3**	**4–8**	**8–16**
NAO	Bab Ounder	S20	1961/1970–1995/2005 1997/2016	2012/13	1996 2012/13	1961/1988 1998/2010	1996/2010
	Tissa	S80	1965/1970–1979–1990–1995/2000 2005/2016	1995/2010	1970 1995	1965 1995/2013	2005/2010
EA	Aknoul	S10	1962/1970–1978 2003/2011–2018	1995	1965 2010	1970/80 2003/2010	1975 1995/2010
	Outat El Haj	S58	1975	1995/2005	1995	1965/1980 2005	1975
WeMO	Aguelman Sidi Ali	S1	1963–1970/1977 2002/2003	1963/1970 2002/2003	1970/2018	1970 1990/2010	1970/75 2005/2010 (>16 years 1970/2010)
	Tafrant	S72	1961/1965–1970/1980 1985/1992–1995 2004 2010/2019	1970 1988	1970 1995	1990/2010	2000/2010

Table 1 shows that the strength and persistence of teleconnection–precipitation coherence vary among these settings: annual and multiyear signals are generally more continuous at wetter stations, whereas drier stations exhibit more intermittent coherence, indicating that the temporal expression of large-scale teleconnections is spatially heterogeneous across the Fez-Meknes region. The frequency analysis highlights the existence of energy bands or coherence at the sub-annual, annual and multi-year scales. Data from the Bab Ounder and Tissa stations have been cross-correlated at the monthly scale with the NAO index. Figure 18 illustrates the result of this operation.

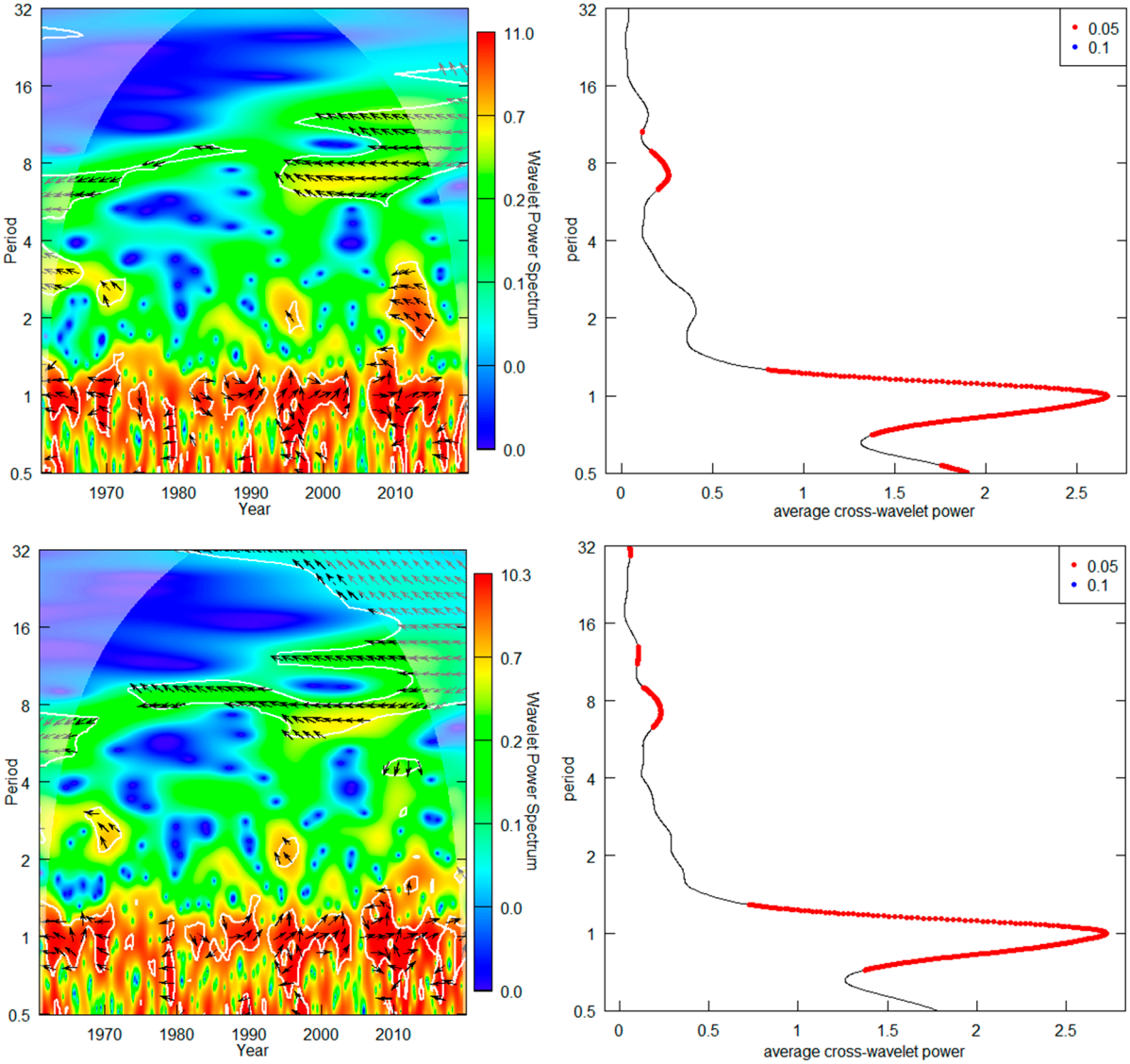


Figure 18. Wavelet coherence analysis between the NAO index and monthly precipitation at the Bab Ounder (**top**) and Tissa (**bottom**). Arrows pointing to the right indicate a positive correlation, those pointing to the left indicate a negative correlation, and areas enclosed in white lines indicate statistically significant correlation. The right-hand panels show the time-averaged cross-wavelet power as a function of period. The black curve represents the average cross-wavelet power; red markers indicate periods significant at the $p < 0.05$ level.

On the annual timescale, a significant energy band reflecting the annual rainfall patterns has been recorded. This pattern is strongly associated with variability in the NAO. Areas of coherence between the two variables appear at 2 years, 6–8 years, and 12 years timescales for the data from the Bab Ounder station. Between 1961 and 1980, the two signals (rainfall and NAO index) are dominantly anti-phase, with a negative correlation (Table 1). After this date (1980),

there are several periods where the two signals become in phase, i.e., a positive correlation, which is unusual but consistent with the trend toward more positive phases in the NAO. The curves on the right of the figure show the average power of the crossed wavelets and the significance level along the frequency domain.

The East Atlantic (EA) pattern considered here is a prominent mode of low-frequency atmospheric variability over the North Atlantic and corresponds to the NOAA/CPC definition based on Barnston and Livezey [21]. Knowing the areas of influence on precipitation amounts within the study area, we chose the two stations Aknoul and Outat El Haj to cross their data with this index. Despite the existence of several areas of consistency between the two series, illustrated in Figure 19, there is a difference in the rainfall variability patterns of the two stations.

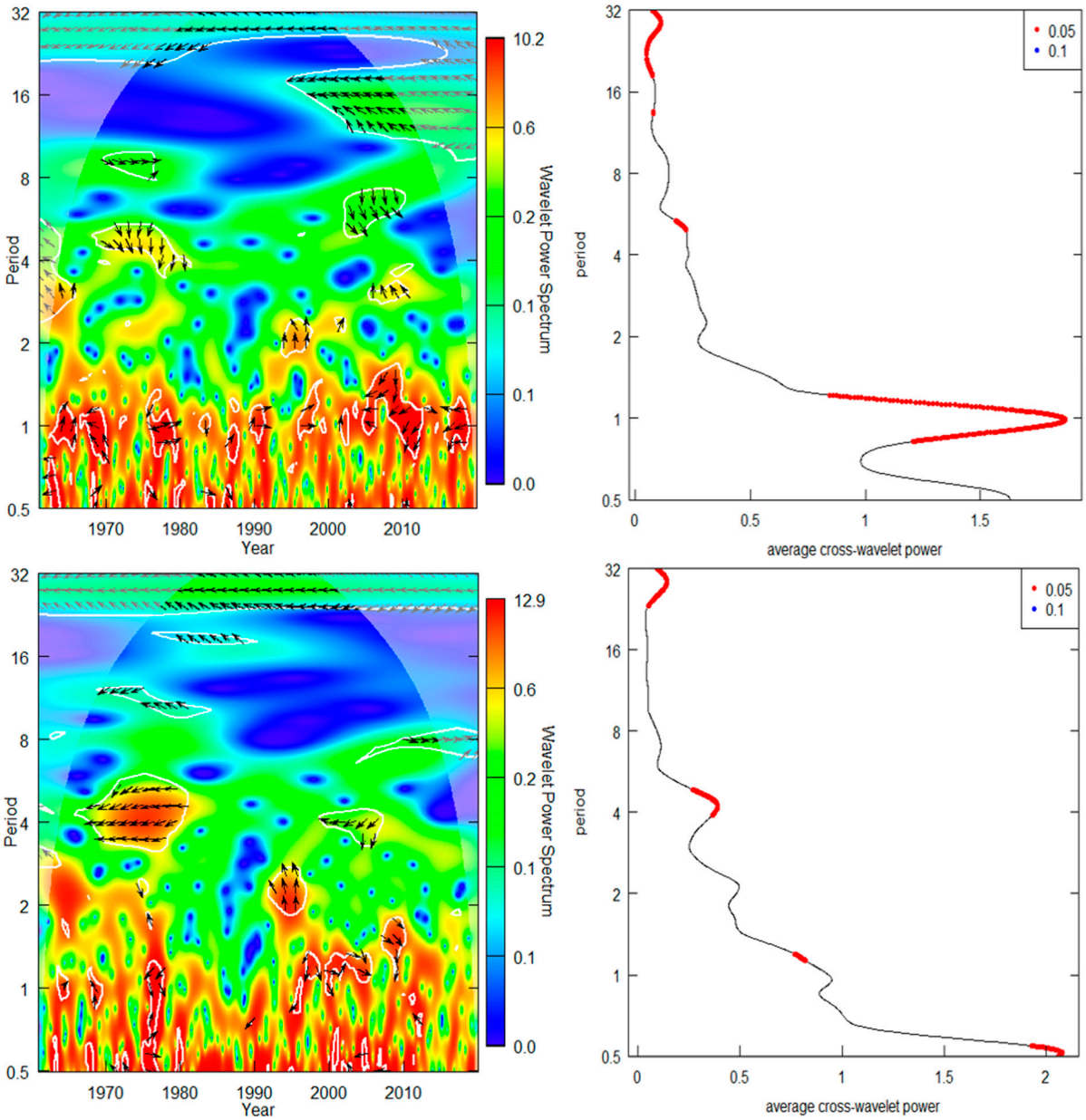


Figure 19. Wavelet coherence analysis between the EAP index and monthly precipitation at Aknoul (**top**) and Outat El Haj (**bottom**). Arrows pointing to the right indicate a positive correlation; those pointing to the left indicate a negative correlation, and areas enclosed in white lines indicate statistically significant correlation. The right-hand panels show the time-averaged cross-wavelet power as a function of period. The black curve represents the average cross-wavelet power; red markers indicate periods significant at the $p < 0.05$ level.

At Aknoul, the annual and sub-annual bands were quite pronounced compared to those of Outat El Haj, which was more arid due to its location in a rain shadow zone. The latter showed only intermittent and discontinuous bands. However, on a frequency scale of 3 to 7 years, the two stations exhibited an anti-phase shift around the years 1970–1980 and 2005. The correlation of rainfall data with the WeMO index revealed significant energy bands at the annual and sub-annual temporal levels, particularly at Tafrant station (Figure 20).

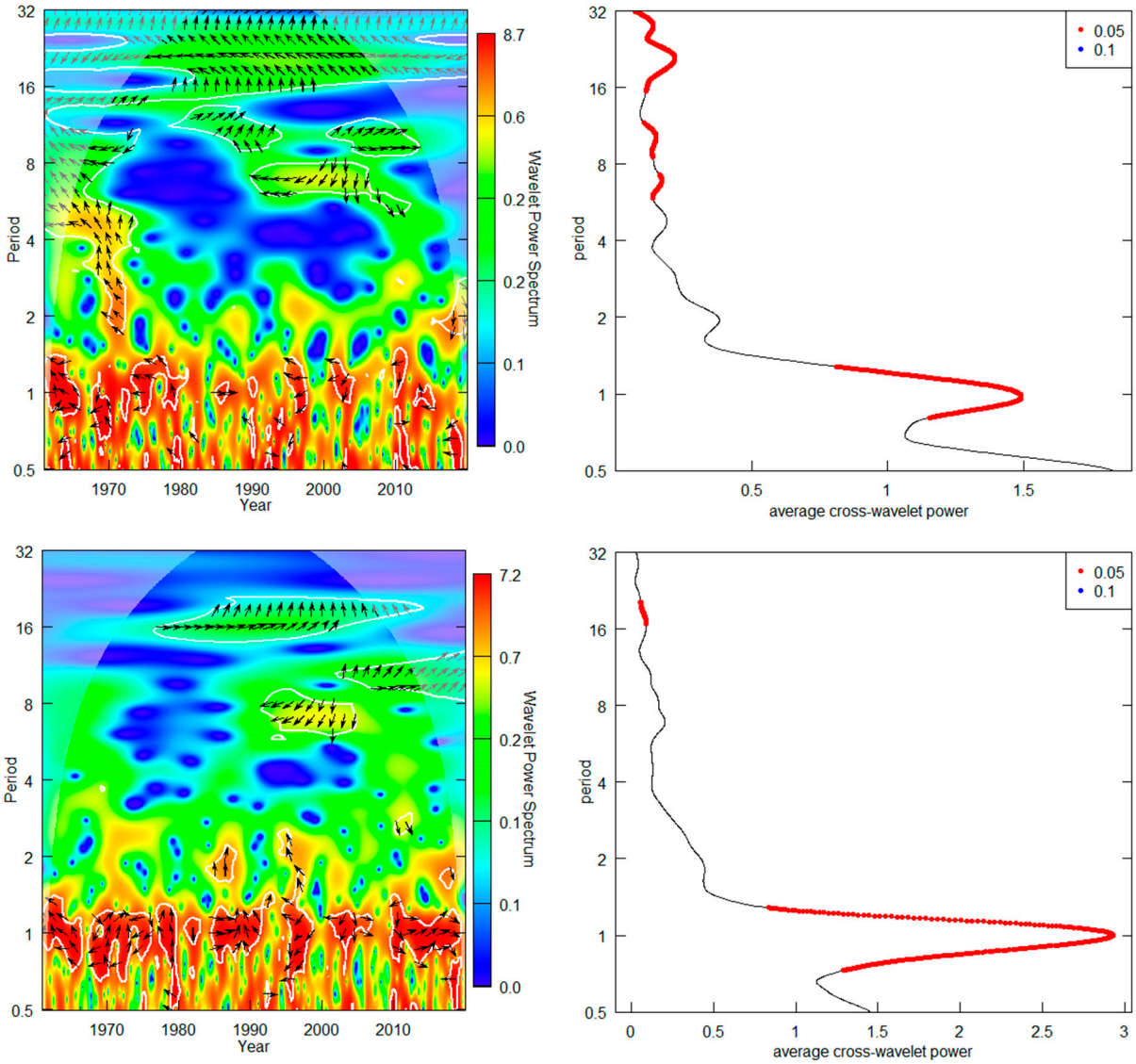


Figure 20. Wavelet coherence analysis between the WeMO index and monthly precipitation at Aguelman Sidi Ali (**top**) and Tafrant (**bottom**). Arrows pointing to the right indicate a positive correlation, those pointing to the left indicate a negative correlation, and areas enclosed in white lines indicate statistically significant correlation. The right-hand panels show the time-averaged cross-wavelet power as a function of period. The black curve represents the average cross-wavelet power; red markers indicate periods significant at the $p < 0.05$ level.

However, the Aguelman Sidi Ali station exhibited a different pattern of variability at the annual level, with discontinuities remaining. By contrast, the low-frequency patterns of variability with periods of 7–10 years and beyond 16 years were similar between the two stations during the period from 1970/80 to 2015 (Table 1).

Table 1 summarizes the main modes of variability revealed by this spectral analysis and according to the climate indices. The periodicities for each index and station were

summarized based on the preceding figures. In particular, the annual timescale showed a fairly strong level of correlation at stations located in the northwestern, wetter part of the study area. However, the stations of Missour and Outat El Haj, located in the Moulouya dry region, exhibited relatively different modes of variability. The modes of precipitation variability with respect to the NAO were similar for Ifrane and Bab Ounder. These stations are wetter. By contrast, the data from the Tissa station, which is moderately drier than Bab Ounder, showed a different mode of variability.

According to the results of this study, the NAO showed stronger correlations with autumn and winter precipitation, which is consistent with the results of Zamrane et al. [55] and Boughdadi et al. [56] regarding the influence of the NAO on rainfall in the study area. Their study also revealed the presence of this annual band of coherence, as well as other multi-annual and multi-decadal modes. The covariance between rainfall at Aknoul and the East Atlantic Pattern (EAP) index is similar to that at Tissa station with the NAO index (Figure 19). However, the interrelationships between rainfall at the Outat El Haj station and this index are completely different, with discontinuities and nuances linked to the arid climate of the upper Moulouya.

The relationship between rainfall and the Western Mediterranean Oscillation (WeMO) is quite strong, especially on the northwestern margins of the region. This relationship is particularly marked in autumn and, to a lesser extent, in winter, thus confirming the results obtained by Hakam et al. [28] and Hakam et al. [57]. However, the relationship of precipitation in the mountainous area with this index differs, showing more pronounced inter-annual and multi-decadal coherences than the annual band, already mentioned in the other cases (Figure 20).

5. Discussion

The findings of this study overlap with those of several others, particularly with regard to NAO associations with precipitation amount. The relationship between rainfall in Morocco and the North Atlantic Oscillation has already been explored by Lamb and Peppler [12] using data from the period 1933–1983. The issue with this study is the integration of several non-Atlantic stations such as Oujda and Midelt within the same standardized precipitation index, in addition to the extended wet season from November to April. The study of Delannoy [13] focused on the Atlantic side of Morocco and was interested in the correlation between precipitation from the previous to the following autumn (excluding summer) and the NAO index of the previous winter. That study found maximum coefficients for the winter season of the order of −0.68 in Taza, −0.55 in Meknes and only −0.18 in Midelt. The issue arising in this case is the grouping of rainfall data from four seasons (fall, winter, spring and the following fall). The share of each season in the annual total is widely different from one station to another; for example, (fall, winter and spring) are 26%, 42% and 30% respectively for the case of Taza, while they are 28%, 20% and 35% in Midelt, affecting the correlations made by Delannoy [13] with the winter NAO index.

The correlations between the NAO index and extreme precipitation in the Mediterranean [58] show their significance over Morocco, especially during the months between December and March, which is in keeping with our results. However, unlike our results, the same study does not present a significant correlation for the autumn months. The studies of Mariotti et al. [59] and López-Moreno et al. [60] also confirm our results on the significant correlations between the NAO index and winter precipitation. According to Seager et al. [61], the fraction of the variance in winter precipitation (DJFM), over the period 1979–2017, explained by the NAO varies between 10% and 40%. Our results are also similar to those obtained by Boughdadi et al. [56] using satellite-derived data, and to those obtained by this recent study of Hakam et al. [57]. The effect of the NAO on precipitation

in the regional climatic context of Morocco (Iberian Peninsula and Maghreb) has been presented in numerous works [62–66].

The relationship between the EAP anomaly and rainfall in Morocco remains to be explored; studies that have addressed this subject are rare. Belaassal [67] is the first study that investigated this issue; he concluded that rainfall in Morocco is well correlated with negative phases of EAP. The work of Hakam et al. [57] also shows this pronounced effect of EAP on spring rainfall. On the other hand, in the Iberian Peninsula, numerous works have been published on this subject. In this context, our results are consistent with those of Rodriguez-Puebla et al. [24], which confirm that the EAP mode has an impact especially on spring rainfall. The significant negative correlations with the EAP index and spring rainfall were also revealed by the work of Kalimeris and Kolios [68], mainly in the central Mediterranean and northwest Tunisia. According to Mellado-Cano et al. [23], the NAO− EA− or EA+ combinations are most linked to the wet condition in our study area, while NAO+ EA− or EA+ are correlated with drought and less rainfall, meaning that the NAO shows the strongest precipitation association among the teleconnection indices considered here. Potentially, the associated negative anomaly of atmospheric pressure during spring might help in the lifting processes responsible for the convective showers and explain links between a negative EAP index and copious rainfall in the study area during this season.

Few studies have explored the relationship between rainfall across Morocco and the WeMO index. The relationship between rainfall in the lower Sebou and the Mediterranean Oscillation (MO) was studied by Hakam et al. [28], who confirmed a significant negative relationship between the MO index and the December precipitation. These results are inconsistent with those of Lopez-Bustins et al. [69] and Gonzalez-Hidalgo et al. [70] on the coasts of Malaga, in the south of Spain. However, the atmospheric configurations responsible for rainfall in this Moroccan-Andalusian zone are very close to each other; this is mostly related to different periods and datasets used. Our results during the winter season coincide with those of Gonzalez-Hidalgo et al. [69], at least for the month of February. López and Frances [71] studied the influence of the WeMO oscillation on atmospheric flows in Spain, and they drew up a map clearly illustrating the areas of influence of the WeMO index; this concerns the entire eastern and southern coasts of the Iberian Peninsula, in addition to areas located in the interior. Boughdadi et al. [27] used satellite-derived rainfall data to investigate the links with NAO and WeMO, showing similar results to ours. The results of Lopez-Bustins et al. [72] agree with our results since they showed that extreme rainfall events in autumn ($\geq$200 mm in 24 h) in Catalonia are associated with a negative WeMO index (≤ -2), especially during the month of October. The WeMO− phases are associated with the passage of low-pressure cells over the Gulf of Cadiz [25]. This cyclonic atmospheric circulation mode brings more autumn precipitation to the Fez-Meknes region.

The cross wavelet analysis on selected stations' data gives us new insights into the relationships between teleconnections and regional rainfall as they might differ over time and at different frequencies. The NAO showed the strongest correlations with autumn and winter precipitation at annual and multiyear scales. The power of coherence is described by the spectral analysis, with a negative correlation or anti-phase before 1980 and a positive or in-phase relationship, but with discontinuities after 1980. The EA pattern showed its strongest correlation with spring rainfall, with similar effects to the NAO index. The WeMO showed its strongest correlation with autumn rainfall over the entire territory.

The most important insight from the spectral analysis is the differences in the behavior of rainfall toward those indices between the wet region in the northwest and that of data from the arid region of Moulouya. The first has an annual band well present in all cases, but in the dry region of Moulouya we record a lot of discontinuities. Our results on the wavelet analysis are consistent with those of Zamrane et al. [55], Addou et al. [54] and

Boughdadi et al. [56], but not those of Hakam et al. [57]. The latter article appears to have some mistakes in presentation, as some graphs, such as those for the NAO, EA, and WeMO index, were incorrectly attributed to the Nino index.

Although several studies have examined the relationships between Moroccan precipitation and large-scale atmospheric circulation indices [73,74], the spatial, seasonal, and temporal structure of these relationships remains incompletely characterized at the regional scale. In particular, previous studies have often focused on individual indices, selected seasons, or individual stations. The present study provides an integrated assessment of the NAO, EAP, and WeMO using a common precipitation dataset and methodological framework across the complete seasonal cycle. In addition to the conventional correlation analysis, we quantify precipitation anomalies associated with the positive and negative phases of each index and examine the temporal and frequency-dependent character of these relationships through cross-wavelet coherence. The spatially distributed dataset also enables comparison between contrasting hydroclimatic environments, from the humid Rif and Middle Atlas sectors to the arid Upper Moulouya. The contribution of the study therefore lies in jointly characterizing the seasonality, spatial coherence, magnitude, and temporal stability of precipitation–teleconnection relationships within one of Morocco's major agricultural regions. The historical relationships identified here may also be relevant for understanding regional sensitivity to future atmospheric-circulation changes. In particular, positive NAO and EAP phases during the study period were generally associated with reduced winter and spring precipitation, respectively. Consequently, future changes in the frequency, persistence, or intensity of these circulation patterns could potentially modify seasonal precipitation regimes in the Fez-Meknes region. However, the present analysis does not include climate projections and therefore cannot determine the future evolution of these teleconnection indices or quantify their future impacts on precipitation. Such questions require dedicated analyses using climate-model simulations and attribution frameworks. Previous studies suggest that Hadley-cell expansion, poleward shifts in mid-latitude circulation, and increasing temperatures may place additional pressure on regional water resources through increased evaporative demand and drought risk [75–77]. However, these future processes are not evaluated directly in the present study. Although more negative WeMO phases are historically associated with higher autumn precipitation, the present analysis does not establish whether such changes would offset possible reductions in winter or spring precipitation.

6. Conclusions

In this study, rainfall gridded data were used to explore links between seasonal precipitation within this region of Morocco and the main atmospheric patterns associated with the climate variability in the western Mediterranean domain.

The principal results of this study can be summarized as follows:

(a) Among the three teleconnection indices examined, the NAO shows the strongest association with autumn and winter precipitation variability in the study area, and a weaker association in spring. More than 97% of the grid cells show nominal local correlations with $p < 0.01$ in winter and autumn. However, the permutation analysis demonstrates that the 389 interpolated grid cells are strongly spatially dependent and represent approximately one effective regional spatial signal; therefore, these percentages describe the spatial coherence of the relationship rather than the number of independent significant locations. Correlation coefficients range from −0.45 to −0.84 in winter and from −0.34 to −0.57 in autumn.

(b) The average increase in rainfall during the negative phases of the NAO is more prominent in winter than in autumn. The decreases during the positive phases of this index

are similar. Spatially, the wet areas (mountains) in the north and the southwest are the most impacted by this change.

(c) The EAP shows its strongest association with spring precipitation, with 95% of the grid cells displaying nominal local correlations with $p < 0.01$. In view of the strong spatial dependence of the gridded field, this percentage reflects the spatial extent of the EAP−precipitation relationship rather than 95% independent significant tests. Furthermore, this index gives us insightful information and explanations about the summer season's scarce rainfall. The percentage (%) change in average spring precipitation according to the EAP+ and EAP− phases matters more in the Upper Moulouya area, with +/−14% to +/−24% than the seasonal averages.

(d) The WeMO shows its strongest association with autumn precipitation, with widespread negative correlations across the study area. The amount of change in the seasonal average ranges between +/−13% and +/−17% according to the WeMO negative and positive phases. The maximum effects of this oscillation are recorded in the Upper Moulouya region and the northwestern tip of the study area.

(e) The cross-wavelet analysis reveals an annual band of energy reflecting the year-to-year variability; multiyear bands with in-phase and anti-phase sub-periods according to indices were also recorded. The differences in the variability patterns between the wet area and dry zone of Moulouya were also characterized.

(f) The historical relationships identified between teleconnection phases and seasonal precipitation may be relevant for drought-risk assessment and regional water-resource planning. However, evaluating their implications for future agricultural systems requires dedicated climate, hydrological, agronomic, and socioeconomic analyses.

Author Contributions: Conceptualization, R.K. and M.H.; methodology, R.K.; software, G.P.; validation, G.P., R.K. and T.C.; formal analysis, R.K.; investigation, R.K. and N.Y.K.; resources, M.H.; data curation, R.K. and G.P.; writing—original draft preparation, R.K. and N.Y.K.; writing—review and editing, A.D.M.; visualization, G.P. and R.K.; supervision, M.H. and T.C.; project administration, M.H.; All authors have read and agreed to the published version of the manuscript.

Funding: This research received no external funding.

Data Availability Statement: The data that support the findings of this study are available on request from the corresponding author.

Conflicts of Interest: The authors declare no conflicts of interest.

References

1. Tuel, A.; Eltahir, E.A.B. Why Is the Mediterranean a Climate Change Hot Spot? *J. Clim.* **2020**, *33*, 5829–5843. [CrossRef]
2. Kmoch, L.; Bou-Lahriss, A.; Plieninger, T. Drought threatens agroforestry landscapes and dryland livelihoods in a North African hotspot of environmental change. *Landsc. Urban Plan.* **2024**, *245*, 105022. [CrossRef]
3. Toreti, A.; Bavera, D.; Acosta Navarro, J.; Acquafresca, L.; Arias Muñoz, C.; Avanzi, F.; Barbosa, P.; Cremonese, E.; de Jager, A.; Ferraris, L.; et al. *Drought in the Mediterranean Region—January 2024*; Publications Office of the European Union: Luxembourg, 2024. Available online: https://data.europa.eu/doi/10.2760/384093 (accessed on 1 September 2026).
4. FAO. Prolonged Drought Significantly Affected 2024 Cereal Production and Delayed Start of 2025 Season. FAO GIEWS Country Brief on Morocco, 6 February 2025. Available online: https://www.fao.org/giews/countrybrief/country.jsp?code=MAR&lang=en (accessed on 1 September 2026).
5. Verner, D.; Treguer, D.; Redwood, J.; Christensen, J.; McDonnell, R.; Elbert, C.; Konishi, Y. *Climate Variability, Drought, and Drought Management in Morocco's Agricultural Sector*; World Bank Group: Washington, DC, USA, 2018.
6. Nigam, S. Teleconnections. In *Encyclopedia of Atmospheric Sciences*; Holton, J.R., Ed.; Academic Press: Cambridge, MA, USA, 2003; pp. 2243–2269. [CrossRef]
7. Misra, V. Teleconnections. In *Regionalizing Global Climate Variations*; Misra, V., Ed.; Elsevier: Amsterdam, The Netherlands, 2020; pp. 143–174. [CrossRef]

8. Hurrell, J.W. Decadal Trends in the North Atlantic Oscillation: Regional Temperatures and Precipitation. *Science* **1995**, *269*, 676–679. [CrossRef] [PubMed]
9. Hurrell, J.W.; Kushnir, Y.; Ottersen, G.; Visbeck, M. An overview of the North Atlantic Oscillation. In *the North Atlantic Oscillation: Climatic Significance and Environmental Impact*; Hurrell, J.W., Kushnir, Y., Ottersen, G., Visbeck, M., Eds.; American Geophysical Union: Washington, DC, USA, 2003; Volume 134, pp. 1–35. [CrossRef]
10. Hurrell, J.W.; Deser, C. North Atlantic climate variability: The role of the North Atlantic Oscillation. *J. Mar. Syst.* **2009**, *78*, 28–41. [CrossRef]
11. Stephenson, D.B.; Wanner, H.; Brönnimann, S.; Luterbacher, J. The History of Scientific Research on the North Atlantic Oscillation. In *The North Atlantic Oscillation: Climatic Significance and Environmental Impact*; Hurrell, J.W., Kushnir, Y., Ottersen, G., Visbeck, M., Eds.; American Geophysical Union: Washington, DC, USA, 2003; Volume 134, pp. 37–50. [CrossRef]
12. Lamb, P.J.; Peppler, R.A. North Atlantic oscillation: Concept and an application. *Bull. Am. Meteorol. Soc.* **1987**, *68*, 1218–1225. [CrossRef]
13. Delannoy, H. Précipitations saisonnières du Maroc cisatlasique et téléconnexions dans la circulation atmosphérique (Seasonal precipitations of the cisatlasic Morocco and teleconnections in the atmospheric circulation). *Bull. Assoc. Géogr. Fr.* **1988**, *65*, 393–406. [CrossRef]
14. Belaassal, A. Précipitations au Maroc et circulation atmosphérique au niveau 700 hPa. *Méditerranée* **1998**, *88*, 19–26. [CrossRef]
15. Knippertz, P.; Christoph, M.; Speth, P. Long-term precipitation variability in Morocco and the link to the large-scale circulation in recent and future climates. *Meteorol. Atmos. Phys.* **2003**, *83*, 67–88. [CrossRef]
16. Born, K.; Fink, A.H.; Knippertz, P.P. Meteorological processes influencing the weather and climate of Morocco. In *Impacts of Global Change on the Hydrological Cycle in West and Northwest Africa*; Speth, P., Christoph, M., Diekkrüger, B., Eds.; Springer: Berlin/Heidelberg, Germany, 2010; pp. 150–163.
17. Driouech, F.; Déqué, M.; Sánchez-Gómez, E. Weather regimes—Moroccan precipitation link in a regional climate change simulation. *Glob. Planet. Change* **2010**, *72*, 1–10. [CrossRef]
18. Sebbar, A.; Badri, W.; Fougrach, H.; Hsaine, M.; Saloui, A. Étude de la variabilité du régime pluviométrique au Maroc septentrional (1935–2004). *Sci. Chang. Planétaires/Sécher.* **2011**, *22*, 139–148.
19. Ilmen, R.; Benjelloun, H.; Ouahmane, L.; Hakkou, M.; Benghazi, M. Étude préliminaire des effets de l'Oscillation Nord Atlantique d'hiver sur les cernes du cèdre de l'Atlas, Cedrus atlantica (Endl.) Carrière, au Maroc. *Bull. Inst. Sci. Rabat* **2016**, *38*, 43–50.
20. Hanchane, M.; El Kassioui, J. Relation entre l'oscillation nord atlantique et les précipitations hivernales au Maroc selon des données récentes (1960–2016). In *Changement Climatique, Potentialités Territoriales et Justice Environnementale*, 1st ed.; USMBA, Ed.; CNRST: Rabat, Morocco, 2021; Tome I, pp. 41–53.
21. Barnston, A.G.; Livezey, R.E. Classification, Seasonality and Persistence of Low-Frequency Atmospheric Circulation Patterns. *Mon. Weather Rev.* **1987**, *115*, 1083–1126. [CrossRef]
22. Wallace, J.M.; Gutzler, D.S. Teleconnections in the Geopotential Height Field during the Northern Hemisphere Winter. *Mon. Weather Rev.* **1981**, *109*, 784–812. [CrossRef]
23. Mellado-Cano, J.; Barriopedro, D.; García-Herrera, R.; Trigo, R.M.; Hernández, A. Examining the North Atlantic Oscillation, East Atlantic Pattern, and jet variability since 1685. *J. Clim.* **2019**, *32*, 6285–6298. [CrossRef]
24. Rodriguez-Puebla, C.; Encinas, A.H.; Nieto, S.; Garmendia, J. Spatial and temporal patterns of annual precipitation variability over the Iberian Peninsula. *Int. J. Climatol.* **1998**, *18*, 299–316. [CrossRef]
25. Martin-Vide, J.; Lopez-Bustins, J.-A. The Western Mediterranean Oscillation and rainfall in the Iberian Peninsula. *Int. J. Climatol.* **2006**, *26*, 1455–1475. [CrossRef]
26. Vicente-Serrano, S.M.; Beguería, S.; López-Moreno, J.I.; El Kenawy, A.M.; Angulo-Martínez, M. Daily atmospheric circulation events and extreme precipitation risk in northeast Spain: Role of the North Atlantic Oscillation, the Western Mediterranean Oscillation, and the Mediterranean Oscillation. *J. Geophys. Res. Atmos.* **2009**, *114*, D08106. [CrossRef]
27. Boughdadi, S.; Saidi, M.E.; Ait Brahim, Y.; Hakam, O.; Rachdane, M. Atlantic and Mediterranean-Sourced Precipitation over the Maghreb: Trends and Spatiotemporal Variability. *Earth Syst. Environ.* **2024**, *8*, 765–782. [CrossRef]
28. Hakam, O.; Baali, A.; Ait Brahim, Y.; El Kamel, T.; Azennoud, K. Regional and global teleconnections patterns governing rainfall in the Western Mediterranean: Case of the Lower Sebou Basin, North-West Morocco. *Model. Earth Syst. Environ.* **2022**, *8*, 5107–5128. [CrossRef]
29. DGCL. *Monographie Générale, Région de Fès-Meknès*; Direction Générale des Collectivités Locales: Rabat, Morocco, 2015; p. 62.
30. Beck, H.E.; Zimmermann, N.E.; McVicar, T.R.; Vergopolan, N.; Berg, A.; Wood, E.F. Present and future Köppen-Geiger climate classification maps at 1-km resolution. *Sci. Data* **2018**, *5*, 180214. [CrossRef] [PubMed]
31. ABHS. Inventaire du degré de pollution des ressources en Eau dans le bassin du Sebou. 2015. Available online: http://www.abh-sebou.ma/wp-content/uploads/2018/02/Brochure-IDP-2013.pdf (accessed on 31 October 2024).
32. Belmahi, M.; Hanchane, M.; Krakauer, N.Y.; Kessabi, R.; Bouayad, H.; Mahjoub, A.; Zouhri, D. Analysis of Relationship between Grain Yield and NDVI from MODIS in the Fez-Meknes Region, Morocco. *Remote Sens.* **2023**, *15*, 2707. [CrossRef]

33. Tramblay, Y.; Koutroulis, A.; Samaniego, L.; Vicente-Serrano, S.M.; Volaire, F.; Boone, A.; Le Page, M.; Llasat, M.C.; Albergel, C.; Burak, S.; et al. Challenges for drought assessment in the Mediterranean region under future climate scenarios. *Earth-Sci. Rev.* **2020**, *210*, 103348. [CrossRef]
34. Tomaszkiewicz, M.A. Future Seasonal Drought Conditions over the CORDEX-MENA/Arab Domain. *Atmosphere* **2021**, *12*, 856. [CrossRef]
35. Kessabi, R.; Hanchane, M.; Guijarro, J.A.; Krakauer, N.Y.; Addou, R.; Sadiki, A.; Belmahi, M. Homogenization and Trends Analysis of Monthly Precipitation Series in the Fez-Meknes Region, Morocco. *Climate* **2022**, *10*, 64. [CrossRef]
36. Kessabi, R.; Hanchane, M.; Caloiero, T.; Pellicone, G.; Addou, R.; Krakauer, N.Y. Analyzing Spatial Trends of Precipitation Using Gridded Data in the Fez-Meknes Region, Morocco. *Hydrology* **2023**, *10*, 37. [CrossRef]
37. Jones, P.D.; Jónsson, T.; Wheeler, D. Extension to the North Atlantic Oscillation using early instrumental pressure observations from Gibraltar and south-west Iceland. *Int. J. Climatol.* **1997**, *17*, 1433–1450. [CrossRef]
38. Olivoto, T.; Lúcio, A.D. metan: An R package for multi-environment trial analysis. *Methods Ecol. Evol.* **2020**, *11*, 783–789. [CrossRef]
39. Kim, J.K. What Is Probability Density Function (PDF) and Cumulative Distribution Function (CDF): How to Calculate Using Excel and R? 2022. Available online: https://agronomy4future.com/archives/16524 (accessed on 25 October 2026).
40. Torrence, C.; Compo, G.P. A Practical Guide to Wavelet Analysis. *Bull. Am. Meteorol. Soc.* **1998**, *79*, 61–78. [CrossRef]
41. Daubechies, I. *Ten Lectures on Wavelets*; SIAM: Philadelphia, PA, USA, 1992.
42. Maraun, D.; Kurths, J. Cross wavelet analysis. Significance testing and pitfalls. *Nonlinear Process. Geoph.* **2004**, *11*, 505–514. [CrossRef]
43. Javanshiri, Z.; Babaeian, I.; Pakdaman, M. Influence of large-scale climate signals on the precipitation variability over Iran. *Stoch. Environ. Res. Risk Assess.* **2023**, *37*, 1745–1762. [CrossRef]
44. Veleda, D.; Montagne, R.; Araujo, M. Cross-Wavelet Bias Corrected by Normalizing Scales. *J. Atmos. Ocean. Technol.* **2012**, *29*, 1401–1408. [CrossRef]
45. Grinsted, A.; Moore, J.C.; Jevrejeva, S. Application of the cross wavelet transform and wavelet coherence to geophysical time series. *Nonlinear Process. Geophys.* **2004**, *11*, 561–566. [CrossRef]
46. Liu, P.C. Wavelet Spectrum Analysis and Ocean Wind Waves. In *Wavelets in Geophysics*; Foufoula-Georgiou, E., Kumar, P., Eds.; Academic Press: San Diego, CA, USA, 1994; Volume 4, pp. 151–166. [CrossRef]
47. Kessabi, R.; Hanchane, M.; Krakauer, N.Y.; Aboubi, I.; El Kassioui, J.; El Khazzan, B. Annual, Seasonal, and Monthly Rainfall Trend Analysis Through Non-Parametric Tests in the Sebou River Basin (SRB), Northern Morocco. *Climate* **2022**, *10*, 170. [CrossRef]
48. Addou, R.; Hanchane, M.; Krakauer, N.Y.; Kessabi, R.; Obda, K.; Souab, M.; Achir, I.E. Wavelet Analysis for Studying Rainfall Variability and Regionalizing Data: An Applied Study of the Moulouya Watershed in Morocco. *Appl. Sci.* **2023**, *13*, 3841. [CrossRef]
49. Born, K.; Fink, A.H.; Paeth, H. Dry and wet periods in the northwestern Maghreb for present day and future climate conditions. *Meteorol. Z.* **2008**, *17*, 533–551. [CrossRef]
50. Kessabi, R.; Hanchane, M.; Ait Brahim, Y.; El Khazzan, B.; Addou, R.; Belmahi, M. Characterization of annual and seasonal rainfall trend using innovative trend analysis (ITA) and classical methods: The case of Wadi Sebou basin (WSB) Morocco. *Euro-Mediterr. J. Environ. Integr.* **2025**, *10*, 555–573. [CrossRef]
51. Isnard, H. La répartition saisonnière des pluies au Maroc. *Ann. Géogr.* **1958**, *67*, 39–42. [CrossRef]
52. Delannoy, H.; Lecompte, M. Utilisation de l'analyse factorielle des correspondances pour l'étude des précipitations quotidiennes: Un exemple au Maroc. *Méditerranée* **1980**, *40*, 29–36. [CrossRef]
53. Addou, R.; Hanchane, M.; Obda, K.; Krakauer, N.Y.; El Khazzan, B.; Kessabi, R.; Achiban, H. Monthly Precipitation over Northern Middle Atlas, Eastern Morocco: Homogenization and Trends. *Appl. Sci.* **2022**, *12*, 12496. [CrossRef]
54. Addou, R. *Hydrologie de l'Oued Melloulou et Changements Actuels: Perturbation des Régimes Climatiques et Pression Anthropique*; Université Sidi Mohamed Ben Abdellah, Faculté des Lettres et des Sciences Humaines Saïs-Fès: Fez, Morocco, 2021.
55. Zamrane, Z.; Mahé, G.; Laftouhi, N.-E. Wavelet Analysis of Rainfall and Runoff Multidecadal Time Series on Large River Basins in Western North Africa. *Water* **2021**, *13*, 3243. [CrossRef]
56. Boughdadi, S.; Ait Brahim, Y.; El Alaoui El Fels, A.; Saidi, M.E. Rainfall Variability and Teleconnections with Large-Scale Atmospheric Circulation Patterns in West-Central Morocco. *Atmosphere* **2023**, *14*, 1293. [CrossRef]
57. Hakam, O.; Bouras, E.H.; Amazirh, A.; Ongoma, V.; Eddamiri, S.; Saidi, L.; Zerouali, A.; Chehbouni, A. Influence of atmospheric and oceanic circulation patterns on precipitation variability in North Africa with a focus on Morocco. *Sci. Rep.* **2025**, *15*, 17977. [CrossRef] [PubMed]
58. Krichak, S.O.; Breitgand, J.S.; Gualdi, S.; Feldstein, S.B. Teleconnection–extreme precipitation relationships over the Mediterranean region. *Theor. Appl. Climatol.* **2014**, *117*, 679–692. [CrossRef]
59. Mariotti, A.; Struglia, M.V.; Zeng, N.; Lau, K.-M. The Hydrological Cycle in the Mediterranean Region and Implications for the Water Budget of the Mediterranean Sea. *J. Clim.* **2002**, *15*, 1674–1690. [CrossRef]

60. López-Moreno, J.I.; Vicente-Serrano, S.M.; Morán-Tejeda, E.; Lorenzo-Lacruz, J.; Kenawy, A.; Beniston, M. Effects of the North Atlantic Oscillation (NAO) on combined temperature and precipitation winter modes in the Mediterranean mountains: Observed relationships and projections for the 21st century. *Glob. Planet. Change* **2011**, *77*, 62–76. [CrossRef]
61. Seager, R.; Liu, H.; Kushnir, Y.; Osborn, T.J.; Simpson, I.R.; Kelley, C.R.; Nakamura, J. Mechanisms of Winter Precipitation Variability in the European–Mediterranean Region Associated with the North Atlantic Oscillation. *J. Clim.* **2020**, *33*, 7179–7196. [CrossRef]
62. Gomes, P.T. Relationships between Iberian Rainfall Variability and the North Atlantic Oscillation. In *Detecting and Modelling Regional Climate Change*; India, M.B., Bonillo, D.L., Eds.; Springer: Berlin/Heidelberg, Germany, 2001; pp. 377–387. [CrossRef]
63. Norrant, C.; Douguédroit, A. Tendances récentes des précipitations et des pressions de surface dans le Bassin méditerranéen/Recent trends in precipitation and sea level pressures in the Mediterranean Basin. *Ann. Géogr.* **2003**, *112*, 298–305. [CrossRef]
64. Trigo, R.M.; Pozo-Vázquez, D.; Osborn, T.J.; Castro-Díez, Y.; Gámiz-Fortis, S.; Esteban-Parra, M.J. North Atlantic oscillation influence on precipitation, river flow and water resources in the Iberian Peninsula. *Int. J. Climatol.* **2004**, *24*, 925–944. [CrossRef]
65. Santos, J.A.; Corte-Real, J.; Leite, S.M. Weather regimes and their connection to the winter rainfall in Portugal. *Int. J. Climatol.* **2005**, *25*, 33–50. [CrossRef]
66. Espinosa, L.A.; Portela, M.M. Rainfall Trends over a Small Island Teleconnected to the North Atlantic Oscillation—The Case of Madeira Island, Portugal. *Water Resour. Manag.* **2020**, *34*, 4449–4467. [CrossRef]
67. Belaassal, A. Variabilité des Géopotentiels à 700 et 500 hPa et Précipitations au Maroc nord Occidental. Ph.D. Thesis, Université d'Aix-Marseille I, Aix-Marseille, France, 2000.
68. Kalimeris, A.; Kolios, S. TRMM-based rainfall variability over the Central Mediterranean and its relationships with atmospheric and oceanic climatic modes. *Atmos. Res.* **2019**, *230*, 104649. [CrossRef]
69. Lopez-Bustins, J.-A.; Martin-Vide, J.; Sanchez-Lorenzo, A. Iberia winter rainfall trends based upon changes in teleconnection and circulation patterns. *Glob. Planet. Change* **2008**, *63*, 171–176. [CrossRef]
70. Gonzalez-Hidalgo, J.C.; Lopez-Bustins, J.-A.; Štepánek, P.; Martin-Vide, J.; de Luis, M. Monthly precipitation trends on the Mediterranean fringe of the Iberian Peninsula during the second-half of the twentieth century (1951–2000). *Int. J. Climatol.* **2009**, *29*, 1415–1429. [CrossRef]
71. López, J.; Frances, F. Influence of the North Atlantic Oscillation and the Western Mediterranean Oscillation in the Maximum Flow. In Proceedings of the International Workshop on Advances in Statistical Hydrology, Taormina, Italy, 23–25 May 2010; pp. 1–11.
72. Lopez-Bustins, J.A.; Arbiol-Roca, L.; Martin-Vide, J.; Barrera-Escoda, A.; Prohom, M. Intra-annual variability of the Western Mediterranean Oscillation (WeMO) and occurrence of extreme torrential precipitation in Catalonia (NE Iberia). *Nat. Hazards Earth Syst. Sci.* **2020**, *20*, 2483–2501. [CrossRef]
73. Xoplaki, E.; González-Rouco, J.F.; Luterbacher, J.; Wanner, H. Wet season Mediterranean precipitation variability: Influence of large-scale dynamics and trends. *Clim. Dyn.* **2004**, *23*, 63–78. [CrossRef]
74. Driouech, F. Distribution des précipitations hivernales sur le Maroc dans le cadre d'un changement climatique: Descente d'échelle et incer-titudes. Ph.D. Thesis, Université de Toulouse III, Toulouse, France, 2010.
75. Lu, J.; Vecchi, G.A.; Reichler, T. Expansion of the Hadley cell under global warming. *Geophys. Res. Lett.* **2007**, *34*, L06805. [CrossRef]
76. Son, S.-W.; Kim, S.-Y.; Min, S.-K. Widening of the Hadley Cell from Last Glacial Maximum to Future Climate. *J. Clim.* **2018**, *31*, 267–281. [CrossRef]
77. Xian, T.; Xia, J.; Wei, W.; Zhang, Z.; Wang, R.; Wang, L.-P.; Ma, Y.-F. Is Hadley Cell Expanding? *Atmosphere* **2021**, *12*, 1699. [CrossRef]

Disclaimer/Publisher's Note: The statements, opinions and data contained in all publications are solely those of the individual author(s) and contributor(s) and not of MDPI and/or the editor(s). MDPI and/or the editor(s) disclaim responsibility for any injury to people or property resulting from any ideas, methods, instructions or products referred to in the content.